HIGH FREQUENCY SIMULATION OF TRANSFORMER WINDINGS FOR DIAGNOSTIC TESTS

by

ARVIND SINGH

B.Sc., The University of the West Indies, 2003

A THESIS SUBMITTED IN PARTIAL FULFILMENT OF
THE REQUIREMENTS FOR THE DEGREE OF

MASTER OF APPLIED SCIENCE

in

THE FACULTY OF GRADUATE STUDIES

(Electrical and Computer Engineering)

THE UNIVERSITY OF BRITISH COLUMBIA

February 2006

ABSTRACT

The change in business dynamics, brought on by the deregulation of the electricity industry has had an impact on the technical operations of the companies involved. To maintain competitiveness, industries must maintain a high level of efficiency and reliability. This has led to the shift to condition monitoring from scheduled maintenance schemes especially for expensive assets which are not immediately replaceable such as power transformers.

High current surges impacting power transformers often cause winding deformations. These pose safety risks and heavy financial losses to the utility in spot market buying when failures occur. Long replacement times can have crippling financial effects on a company if there is no replacement for the transformer when a failure occurs. As a result of this diagnostic methods which estimate the transformer condition have become increasingly important. These allow personnel to make decisions on replacing or relocating a power transformer, in keeping with the financial objectives of the company.

In this report an overview of the methods used in obtaining winding signatures used for condition monitoring is presented. An equivalent circuit winding model based on multiphase transmission line theory is developed which includes enough detail to allow for an accurate simulation. The circuit model for a specific transformer winding was implemented using Microtran software. The model was used to compare the response of the commonly used transadmittance signature to the characteristic impedance signature of the winding for different types of deformations (simulated by changing different capacitances in the model).

It was found that the methods were comparable in sensitivity with the transadmittance being only marginally better. The characteristic impedance signature however had the advantage of showing a constant percentage change over its frequency range for a given distortion. This makes it easier to quantify winding movement. The use of both methods in conjunction may serve as a more efficient method of classifying physical winding changes.

TABLE OF CONTENTS

LIST OF TABLES

LIST OF FIGURES

ACKNOWLEDGEMENTS

INTRODUCTION

SHIFT IN ENERGY ECONOMICS

Traditionally, Electric utilities were corporate monoliths. In most cases they existed as state owned monopolies. These could, for the most part, pass their losses directly on to their customers who had little choice but to accept the quality of service with which they were provided. Recently this economic model of vertically integrated utilities was replaced by multiple corporate entities. These provide unbundled services and employ market-driven decisions. In theory, this would give more power to the consumer by giving them a choice, much in the same way the telecommunications industry now operates.

A network of energy generation companies has to make their product available through shared infrastructure, namely the electricity grid. The health of this grid can be severely affected by any independent power producer. Companies may incur heavy expenditures when other companies are affected by problems caused by them. In addition they may have to purchase power from other companies to fulfill their contractual agreements. It therefore becomes necessary to pay more attention to the state of critical assets and infrastructure. At the same time however, they must maintain competitive prices in order to survive financially and so cannot afford to replace equipment on a regular schedule.

These competitive business dynamics have emphasized the need for proper and effective asset management schemes. Asset management can be broadly defined as the balancing of performance, cost and risk in order to maximize returns for the company. It requires proper alignment of corporate goals and management and technical decisions. It involves business processes and information systems that are able to make consistent and beneficial decisions on asset-level data. The general consensus among experts is that the key to optimizing the use of assets is minimizing the risk of failures and their effects.

Power transformers are the most expensive and most complex assets in substations. Outages due to power transformer failure cost the company money not only in replacement or repair costs but also in buying power from other companies to supply their customers, in environmental clean up costs, customer and collateral damage costs and increased insurance premiums. These costs can quickly run into millions of dollars in the space of just a few days. A case study carried out by Pacificorp [1] estimated the failure of a 520MVA transformer to reach US$17 Million in just 8 days. The following break down was given:

Equipment costs: $3.5 Million

    Transformers: **3 Million**

    Collateral Equipment damage

    Environmental clean up: **$0.5 Million**

Company Losses

    Self-insured deductible: **$1 Million**

    Environmental clean up **$0.5 Million**

    Replacement Power on Spot market **$1.5 Million per DAY**

$100 per MWH spot market price

$30 per MWH continuing production cost

500MW purchased on the spot market

Total cost to purchase power = 500x(100+30)x24hrs

=$1.56 Million per day

Other important factors motivating the adoption of continuous monitoring systems for such critical assets such are high equipment costs and long replacement lead times. Power transformers cannot be bought off the shelf, and in general, because of their size, and cost and lifetime, back up units are not stored by companies. In some cases the replacement process may extend over a year. Given the heavy financial losses that can be incurred by an unexpected failure, traditional time based maintenance schemes have become untenable. As the estimated lifespan of the majority of in service power

transformers is approached, condition based monitoring techniques are becoming more integral to power system operations.

CHAPTER OUTLINE

The report is organized in the following chapters:

CHAPTER 1: TRANSFORMER FAILURE

This section defines transformer failure in the traditional sense as well as in the sense of condition monitoring schemes. An overview of the general causes of transformer failure is given with specific focus on the failures related to winding movement.

CHAPTER 2: WINDING DISPLACEMENT

This section outlines some of the principal causes of winding deformations especially those arising from high current conditions.

CHAPTER 3: DIAGNOSTIC METHODS

This section outlines comparison methods as well as common winding signatures used in practice with particular attention being paid to the "Frequency Response Analysis" (FRA) technique

CHAPTER 4: THE TRANSMISSION LINE DIAGNOSTICS (TLD) METHOD

This section introduces the concept of traveling waves and develops the theory on which the TLD method is based.

CHAPTER 5: TRANSFORMER MODELLING

This section presents considerations for developing a sufficiently detailed equivalent circuit transformer model based principally on the geometry of the transformer. The main features of the software developed for building the equivalent circuit transformer model are also presented.

CHAPTER 6: MEASUREMENT AND MODELLING ISSUES

This section looks at errors arising from measurement issues such as the effect of standing waves and model issues such lumping of resistances are investigated. A look at phase 'error' introduced by using multiphase elements is also presented.

CHAPTER 7: COMPARISON OF TLD AND FRA METHODS

In this section the transformer circuit model developed is used to simulate different types of fault conditions and to compare the changes obtained from the characteristic impedance and trans-admittance signatures.

CHAPTER 8: DISCUSSIONS

General comments on the results obtained and proposal for further work

CHAPTER 9: CONCLUSIONS

CHAPTER 1: TRANSFORMER FAILURE

1.1 INTRODUCTION

This section defines transformer failures in the traditional sense as well for condition monitoring schemes. An overview of the general causes of transformer failure is given with specific focus on the failures related to winding movement.

1.2 FAILURE DEFINITIONS

Traditional (Critical Failure) definition

A transformer is said to have failed when it is forced out of service by a specific event that results in the inability of the transformer to operate properly under nominal system conditions. Only the present state of the transformer is considered in deciding whether to keep the transformer in service or not. That is, the transformer is considered to be operational as long as it can operate under normal operating conditions.

Preventative (Non-critical Failure) definition

A transformer is said to have failed when it can no longer withstand the fault conditions for which it was originally designed. This means that the transformer may be operable in the traditional sense but could be classified as having failed because the next fault condition would cause it to fail. It entails assessing how "fit" the transformer is and making a decision as to whether it is safe to operate based not only on its present condition but on the probability of catastrophic damage occurring by abnormalities that are likely to happen in the normal course of operation.

1.3 GENERAL CAUSES OF TRANSFORMER FAILURE

The behaviour of a transformer depends on the physical state it is in, that is, the arrangement (shape, symmetry etc) of the windings, and the condition of the insulation (both paper and oil). When transformer ratings are specified, they relate to the voltages that the dielectrics can withstand before breakdown and the short circuit forces that can be endured by the structures that hold the windings in place. It follows therefore that transformer failures stem from exceeding of the withstand capabilities in these categories.

The transformer can be looked at as a combination of three systems: electrical, mechanical and chemical. Figure 1 gives an overview of how these interact during over current conditions.

High current, magnetic fields lead to high forces, expansion and contraction due to heating

Mechanical System

Change in winding arrangements, Insulation thickness

Heating
Electrolysis
Pyrolisis

Non-uniformities

Electrical system

Thermal / Chemical System

Change in dielectric causes change in circuit parameters like capacitance

High currents lead to heating,
High electric field strength lead to dielectric breakdown

Figure 1: Overview of processes taking place during a severe fault condition

When these processes operate they always lower the strength of the transformer to future over-current events as shown in Figure 2.
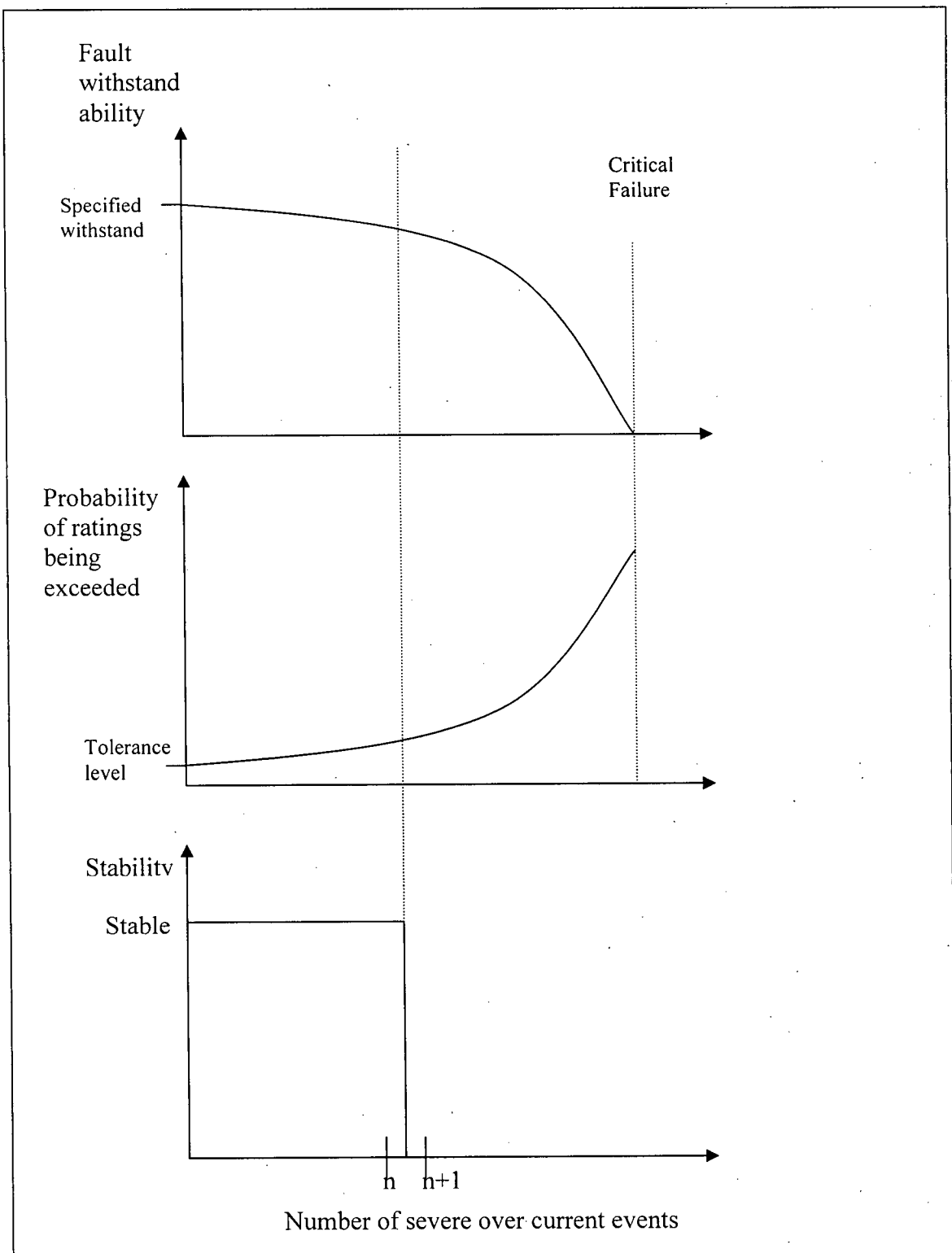
Figure 2: Effect of severe fault conditions on withstand ability

In the normal course of operation, the physical state of the transformer is stable. This means that the elastic limits of the clamps and windings have not been exceeded and the dielectrics have not broken down in any area. When a severe fault occurs that causes these elastic limits to be exceeded or the dielectrics to break down, then plastic deformation of windings or chemical changes in the insulation take place respectively.

The transformer does not return to its pre-fault physical state but moves to a new state instead. For example, clamps may be slightly stretched thus reducing the clamping pressure after the fault is cleared or gasses may be liberated in the oil. This new state that the transformer moves to has an altogether different set of ratings associated with it. As long as the new set of ratings is still acceptable then the transformer can be kept in service. If not taken out of service, the transformer can reach an unstable state where new dynamics have to be taken into consideration (e.g. vibrations of the winding if the clamp has been sufficiently loosened). In the normal course of operation, the state may continue to degrade till the transformer completely collapses.

Traditionally as long as the transformer was stable (up to 'n' faults on Figure 2) then it would be kept in service till the next scheduled maintenance time. However, in order to avoid critical failures the transformer has to be taken out of service at the "nth" short circuit at the latest in order to prevent the system going to an unstable state. Since the ratings decrease with the number of severe faults encountered then the probability of the new ratings being exceeded in a given time increases correspondingly and the time between severe over current events decreases.

The final mechanical or insulation breakdown of a transformer may be due to a number of primary causes. These include: presence of oxygen and/or moisture, solid contamination of the oil, manufacturing defects, transients due to lightning or switching, internal winding resonance, faults and overloads.

Several methods have been developed [2] over the years that can give some insight into the condition that the transformer is in. These include: Frequency Response Analysis (FRA), Dissolved Gas-in-oil Analysis (DGA), ratio measurements, winding resistance, short circuit impedance and loss, excitation loss and dissipation factor, capacitance and applied and induced potential. Among these methods FRA and DGA have emerged as the main methods of transformer diagnostics.

Although the primary causes of transformer failure have been mentionedd, they do not necessarily give direct insight into the physical state of the transformer. This is needed to determine how "fit" it is. In order to get this insight, measurable effects such as insulation degradation, change in oil properties and winding displacements have to be examined. A survey, [3], found that between 70 and 80% of failures can be traced back to short-circuit between winding turns. Table 1 shows that winding displacements can be associated with a number of different primary causes that account for a high percentage of transformer failures.

	1975	1983	1998	Winding movement evident
Lightning Surges	32.3%	30.2%	12.4%	YES
Line Surges/External Short Circuit	13.6%	18.6%	21.5%	YES
Poor Workmanship-Manufacturer	10.6%	7.2%	2.9%	YES
Deterioration of Insulation	10.4%	8.7%	13%	
Overloading	7.7%	3.2%	2.4%	
Moisture	7.2%	6.9%	6.3%	
Inadequate Maintenance	6.6%	13.1%	11.3%	YES
Sabotage, Malicious Mischief	2.6%	1.7%	0	
Loose Connections	2.1%	2.0%	6%	YES
All others	6.9%	8.4%	24.2%	

Table 1: Sources of Transformer failures and causes of winding displacement [4]

From Table 1 it is possible to calculate that the average of failures related to winding displacement is 63.5% for the three years and 54.1% for the latest year (1998). Table 2 shows an excerpt from "Electricity Today" [5] outlining the percentage of transformer failures by component.

Transformer Component	Percentage of failures component is responsible for
High Voltage Windings	48%
Low Voltage Windings	23%
Bushings	2%
Leads	6%
Off-load Tap Changers	0%
Gaskets	2%
Other	19%

Table 2: Transformer failures by component [4]

From the table, just over 70% of transformer failures are due to winding related trauma. In fact the only element that causes more failures than the transformer windings are the on-load tap changers (not shown in Table 2) present in some transformers. These account for 41% of failures in transformers containing them while winding related failure accounts for approximately 19%.

CHAPTER 2: WINDING DISPLACEMENT

2.1 INTRODUCTION

The mechanical structure of a transformer may be compromised by a number of causes including: poor handling during transportation, poor manufacturing, natural ageing or over-current conditions brought on by system faults or lightning. This section briefly addresses the problems arising out of these conditions.

2.2 GENERAL CAUSES OF WINDING DEFORMATION

Natural Ageing

Under normal operating conditions the components of the transformer will slowly deteriorate. The insulation will gradually lose its elasticity and may begin to crumble, clamps will loosen, and generally the structure undergoes a gradual weakening.

Poor manufacturing or maintenance

Lax quality control in the manufacturing process can lead to a number of undesirable conditions such as loose brackets which lead to winding vibration, non-uniform surfaces which contribute to accelerated insulation break down and may lead to internal corona and partial discharge, oil impurity, and short circuit between turns. During maintenance it is not unheard of for equipment to be mistakenly left in the transformer tank. Many times these items would be magnetic materials that get pulled around the tank by the strong magnetic fields of the transformer under normal operation. When these collide with the windings they can quickly destroy insulation and cause short circuits

Short Circuit Forces

Given that standards in transit, manufacturing and maintenance have been upheld it is high current conditions that are the most serious threat to the transformer's structure. Under high current conditions, the transformer can undergo stresses over 100 times the forces it was designed to withstand. Consider a current surge entering one of the terminals of the transformer, distortion can be caused along two main directions:

1. Radial
2. Axial

Radial Movement
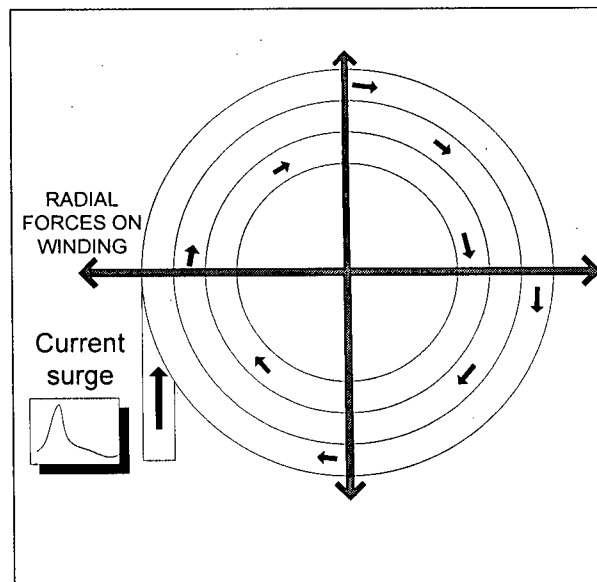
Figure 3: Radial forces due to Current surge

The transient forces on the winding can exceed 100,000lbs in transformers as small as 10MVA [6] and are the principal source of winding deformation. This type of deformation is most dangerous because it has the ability to loosen and deform clamping structures. If this is left unchecked it can result in the entire winding structure coming apart with explosive results. This type of deformation also stretches the insulation and may cause cracks or brittleness and speeds the rate at which it naturally deteriorates.

Axial movement

Axial movement is brought about by the non-uniform energization of the winding which induces radial flux. Consider the steady state flux orientation of the windings as shown in Figure 4.
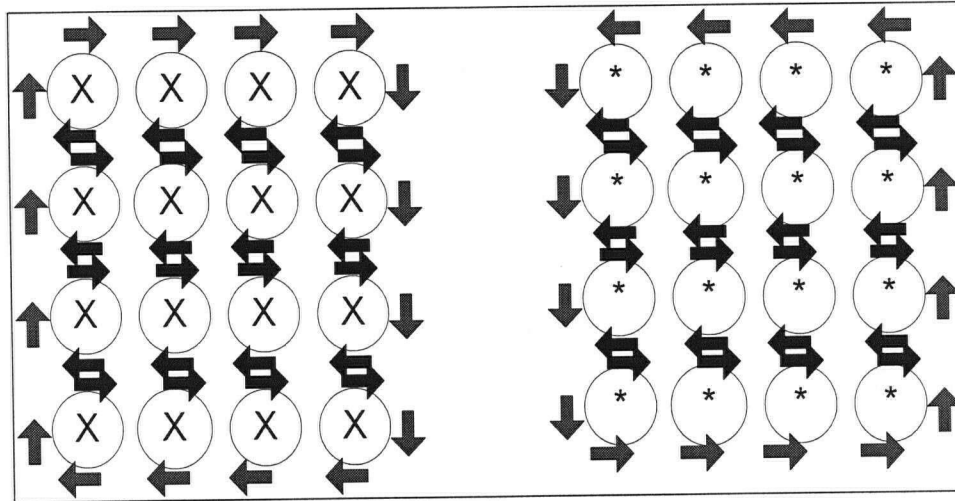
Figure 4: Steady state flux orientation of winding

The grey arrows represent net flux directions while the solid black arrows show fluxes that have been cancelled by the arrows next to them. There is no net magnetic field inside the winding arrangement because the internal fields cancel each other. However, when a fast surge impacts the coil the majority of the current wave may be confined to a few windings or layers at a time and as such the surrounding windings experience net radial fluxes as shown in Figure 5 .
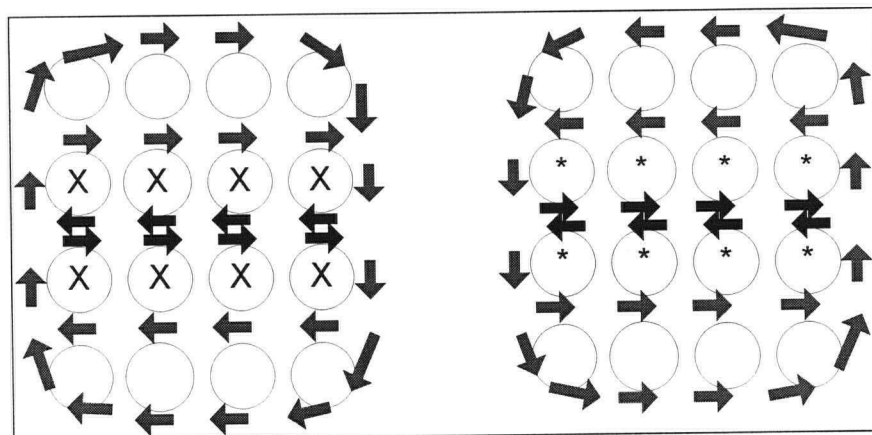
Figure 5: Radial flux experienced due to fast surges

This type of flux causes axially compressive forces to be exerted on the winding. In addition, the flux directions though principally axial may also have some radial components. These types of forces can cause the twisting of windings in addition to compression. This can result in rapid breakdown of insulation between layers leading to short circuits or partial discharge. Gases may become liberated in the oil, some of which are explosive, such as hydrogen. This represents a serious safety concern to both personnel and equipment.

CHAPTER 3: DIAGNOSTIC METHODS

3.1 INTRODUCTION

Methods to diagnose the condition of power transformers have become important tools for electrical utilities in recent years. The need for them arises from two main factors:

1. The majority of power transformers in service are approaching their life span so there is an increased risk of mechanical failure.

2. The operation of deregulated markets requires the use of critical assets to be optimized. This means transformers have to run as long as possible at their limits.

The general principles involved in diagnosing the condition of windings are examined in this section.

3.2 COMMONLY USED WINDING DIAGNOSTIC METHODS

The choice of diagnostic method used to estimate the condition of a winding is dependent on a number of criteria including:

- Sensitivity to winding displacements
- Sensitivity to noise
- Sensitivity to measurement set up
- Ability to diagnose and quantify type of deformation

Some of the most common methods to evaluate the state of a transformer are the following:

Visual inspection

Visual inspection is the most reliable method to determine the winding condition. The transformer has to be taken out of service, drained and opened up to be inspected, the condition of clamps, windings and insulation can then be inspected to determine if there are any noticeable problems. This method requires trained and experienced personnel to carry out inspections and can lead to long out of service times for the transformer which is undesirable. This method is likely to be retained only as a final verification when a less invasive method detects the presence of a critical fault condition.

Short circuit impedance

The low voltage winding terminals are shorted to each other and the input current voltage and power are measured. A deviation of 2% or greater is considered to be indicative of significant winding movement. This technique has to be performed offline in a test lab and is only effective for significant winding distortion.

Leakage reactance test

The short circuit impedance test set-up can also be used to calculate the new leakage reactance of the transformer. If the winding has expanded, the leakage reactance would increase as a consequence. This method is sensitive to certain types of distortion only, namely distortion that results in increased distance between the primary and secondary coil. It does not pick up distortions such as twisting of windings and is ineffective at high frequencies due to the skin effect.

Winding ratio test

The winding ratio test is another offline test that can be used to detect faulty winding conditions. The transformer's voltage ratio is tested to ensure that the proper turns-ratio is present. This can be used to detect short circuited or open circuit conditions.

Winding resistance test

The winding resistance test is also an offline method. It operates on the principle that any change in the geometry of the conductor would show up as a change in the winding resistance. For example if the winding expands then the length of the winding would increase while the cross sectional area would decrease. This would cause an increase in the resistance of the winding. The technique requires highly sensitive equipment to detect fraction of an ohm changes. In addition since the temperature at which the experiments are carried out would influence the quality of the readings, temperature information has to be recorded as well to ensure repeatability when conducting future experiments.

Vibration test

Vibration testing involves the mounting of acoustic sensors on the tank wall of the transformer to sense the vibration of the transformer caused by the continuous magnetization and demagnetization of the core and windings. These acoustic signals

form the signature for the winding. This method has the advantage of being an online method; however the externally mounted sensors are highly susceptible to vibration noise from the external environment.

3.3 COMPARISON TECHNIQUES

Transfer function signatures have become somewhat of an industry standard for transformer diagnostics, especially where the condition of the windings are concerned. The general approach to transfer function diagnostics is the comparison of a given transfer function of the transformer to a base signature that represents the transformer in a healthy condition. The current signature of the transformer can be obtained by measurements on the actual transformer. The base signature, however, is more difficult to acquire. Over the past few years three methods have been used to generate base signatures for power transformers [7]:

1. Temporal signatures
2. Construction based signatures
3. Type based signatures

Figure 6 illustrates the differences in these methods
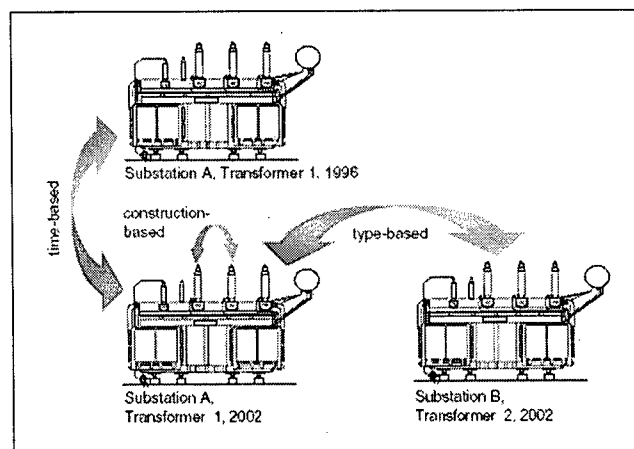
Figure 6: Illustration of time, construction and type based comparisons [7]

Temporal Signatures

Temporal signatures are simply the signature of the transformer obtained at an earlier date. This is the most reliable signature that can be used. When the transformer is new the signature is recorded and this serves as the reference for all future measurements. This data is usually not available though, since transformers have been in service for decades while condition monitoring techniques are relatively new. This means that alternate methods for obtaining baseline signatures usually have to be employed.

Type based signatures

Type based signatures involve obtaining a signature from an identically constructed transformer that is known to be in good condition. This may typically be a relatively new transformer that has been installed at another substation or one that services a low fault area so that the only change in transfer function would arise from natural ageing. The main problem with this method is that even for identically specified transformers, winding designs over time may have changed, causing slightly different transfer functions, in addition, designs are made within a certain tolerance level so that there would be slight variations from one transformer to the next even if the winding designs used are identical. To solve this problem Christian and Feser [7] have proposed the statistical calculation of tolerance bands using transfer functions from a large group of same-type transformers to distinguish differences arising from winding distortions to differences arising from different manufacturing processes.

Construction based signatures

Construction based signatures are used on multi-leg transformers where windings are not zigzag connected. The process entails using the windings on different legs as mutual references. Each winding is tested separately and then transfer functions compared. Christian and Feser [7] find that the geometrical properties of the core-and-coil assembly as well as the type of vector group have noticeable effects on the comparability of the results of different legs. The approach is not constrained to three-phase transformers, where three single phase transformers are used the technique is equally viable. The technique of using windings as mutual references has the advantage of

19

requiring no past or external data for measurement. Measurements [7] show that the frequency responses of three windings are near identical.

The technique has the following advantages: the problem of different manufacturing techniques does not affect it since the windings are part of the same unit. Past data is not needed since asymmetries are evident from comparison of present data. Unless a three phase fault that symmetrically distorts all the windings occurs, which almost never the case, winding movement and distortion can always be ascertained.

The disadvantage of the technique is that if the three windings undergo change in their frequency response characteristics then the asymmetry would give misleading results, making the winding look like it has moved more or less than it actually has.

3.4 FREQUENCY RESPONSE ANALYSIS (FRA)

Frequency response analysis involves measuring the trans-impedance or trans-admittance of the winding. This method has come to be somewhat of an industry standard, because of its high sensitivity to a number of different types of winding distortion. This method is based on the fact that a change in winding geometry results in a change of the RLC parameters of the winding. This results in the magnitudes and frequencies at which resonances occur to also change. There are two methods that are typically used to carry out the FRA measurements:

1. Swept Frequency
2. Low Voltage impulse

Swept Frequency

Swept Frequency Frequency Response Analysis (SFRA) involves injecting a sinusoidal voltage into one end of the winding and then measuring the output current at the other end. The transadmittance is then calculated from the phasor quantities. This is repeated for a wide range of frequencies to obtain the transadmittance signature. White noise is also sometimes used as an injected quantity, since it contains all frequencies at equal power levels. The Fourier transform is then applied to the input and output measurements to obtain their phasor form representations and finally the transadmittance is calculated.

$$Y = \frac{fft(I_{out})}{fft(V_{in})}$$

Low Voltage Impulse

The Low voltage impulse method or (FRA-LVI) involves injecting a low voltage pulse at the input and recording the current at the output terminal. The input and output waveforms are then processed in the same way as is done with white noise in SFRA measurements.

There has been much debate about which of these methods is actually better. Tenbohlen and Ryder [8] have explored the relative advantages and disadvantages of the methods, which are summarized below. They conclude that SFRA is the superior method.

21

SFRA Advantages	FRA LVI Disadvantages
• High signal to noise ratio • Wide frequency range • Adaptable frequency increments (better resolution at low frequencies) • Only one piece of measuring equipment needed (Network analyzer)	• Signal to noise ratio decreases with frequency as higher frequency components have less energy. • Frequency resolution is fixed and poor at low frequencies • Several pieces of equipment needed (function generator, rogowski coil, digital oscilloscope) • Difficult to filter out broad band noise

SFRA Disadvantages	FRA LVI Advantages
• Time taken to make each measurement is relatively long (several minutes)	• Time taken to make each measurement is short (typically one minute).

Table 3: Comparison of SFRA and FRA-LVI according to Tenbohlen and Ryder

Jeffery A. Britton of Phoenix technologies has also compared these methods [9] and has put forward the following comparisons

SFRA Advantages	FRA LVI Disadvantages
• Intuitive and straightforward	• Sensitive to noise can have a drastic effect on transfer function results • Repeatability not of a high standard without the use of very expensive equipment

SFRA Disadvantages	FRA LVI Advantages
• Network analyzer traditionally used which does not have sufficient power to appreciably excite windings at high frequencies due to large inductive load. • Insufficient power to excite windings at very high frequencies due to high capacitive load of insulation system. • Low level signals result in high measurement errors and poor repeatability especially on high current windings. • Extremely sensitive to measurement set up since cable lengths may exceed 50 feet.	• Voltage and currents measured at the transformer, thus minimizing the effect of the external circuit setup. • Low inductance shunts may be used to reduce damping compared to 50 ohm internal impedance of network analyzer in SFRA.

Table 4: Comparison of SFRA and FRA-LVI according to Jeffery A. Britton

The comparisons show that the main downfall of SFRA relates to the equipment used to take measurements. If it were possible to take measurements at the transformer terminals with a sufficiently strong signal then SFRA would clearly be a better option for diagnostics. Since the Transmission Line Diagnostics (TLD) technique described in the next section utilizes the same measurements as SFRA and takes them at the transformer terminals, it is assumed that the SFRA would indeed be the superior choice to FRA LVI for comparisons.

Ryder, proponent of SFRA, describes [10] the key indicators of damage when comparing SFRA signatures as:

- Changes to the overall shape of the graph.
- The creation of new resonant frequencies or the elimination of existing resonant frequencies.
- Large shifts in existing resonant frequencies.

Through a series of case studies he put forth the information in table 5 regarding the ability of FRA to detect fault conditions.

Nature of Fault	Detectable?
No core earth	Probably not detectable except under laboratory conditions.
Multiple core earths	Usually not detectable
Foreign object	Not detectable.
Additional turns on yoke Additional turns on limbs	Detectable. Detectable.
Short-circuited turns	Detectable.
Mechanical damage to windings -to core	Detectable. Detectable if very severe.
Windings unclamped	Probably not detectable except under laboratory conditions.
Loose turns	Detectable.
"Normal" ageing	Detectable if very severe.

Table 5: Ability of FRA to detect various types of faults

As stated earlier, FRA has become somewhat of an industry standard due to its sensitivity, however the quantification of the differences in the transfer function and extracting insightful information about the nature of the winding deformations from these differences are still being researched. Solutions varying from neural networks to simple correlations have been used to different degrees of success.

CHAPTER 4: THE TRANSMISSION LINE DIAGNOSTICS METHOD

4.1 INTRODUCTION

This proposed method [11] relies on the use of the frequency-dependent characteristic-impedance of the transformer as its signature. It arises out of the conceptualization of the winding as a traveling wave medium on which voltage and current waves propagate. When energy is input to the medium, the energy goes toward developing magnetic and electric fields. The rate at which these fields are developed, as well as the quantity of flux that is produced both influence the propagation characteristics. The magnetic fields can be represented by circuit inductance while the electric fields can be represented by circuit capacitance. Both of these are directly related to the geometry of the winding so winding displacements will be reflected in the changes in propagation characteristics.

4.2 TRAVELING WAVES ON TRANSFORMER WINDINGS

Traditionally, traveling wave theory has been used in transient simulations for long lines (>150km) when lumped parameter models no longer give accurate results. The winding of a power transformer however has been estimated to be between 1.5 and 2km long. This may seem very short even for a short line model (<40km), however, the fact is that energy is always transmitted as traveling waves. The lumped parameter model arises when the speed at which the energy propagates is very much greater than the rate at which the energy level changes. Another way of looking at this is that the wavelength of the applied signal is much greater than the length of the line (see Figure 7).
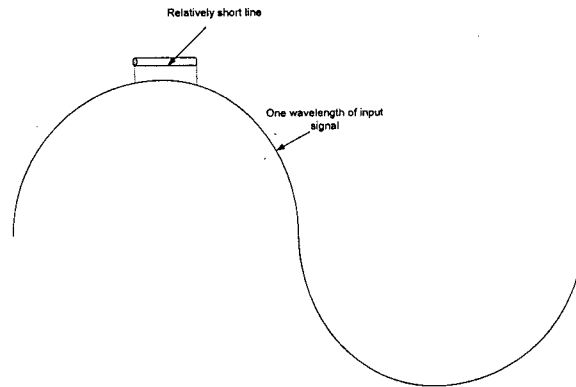
Figure 7: Illustration of Lumped Parameter approximation

Figure 7 shows that the whole winding sees approximately the same potential. For a given length of winding the lower the frequency of the input signal, the better the lumped parameter approximation becomes, or vice versa. When the length of the winding becomes long compared to the wavelength of the line, the situation illustrated in Figure 8 arises.
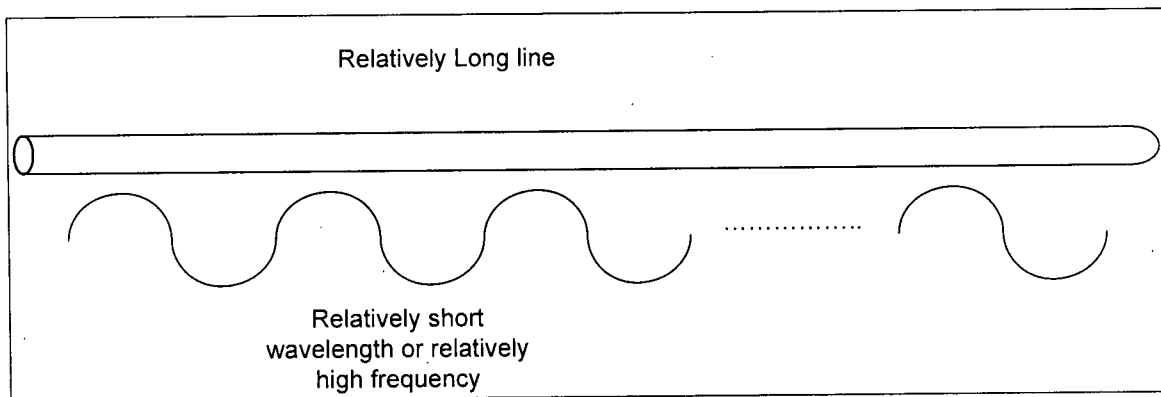
Figure 8: Illustration of high frequency wave on a transmission line

The speed at which the energy propagates is no longer sufficient to assume that the line is at a single potential and therefore one end of the line may be at an altogether different potential to the other end.

This means that although lumped parameter networks are sufficient for modeling transformer windings at low frequencies such as power system frequencies of 60Hz, at high frequencies in the megahertz range, this approximation becomes invalid. At these

frequencies pulses applied to the transformer would not be seen by the whole winding at the same time by instead propagate down the winding as shown in Figure 9.
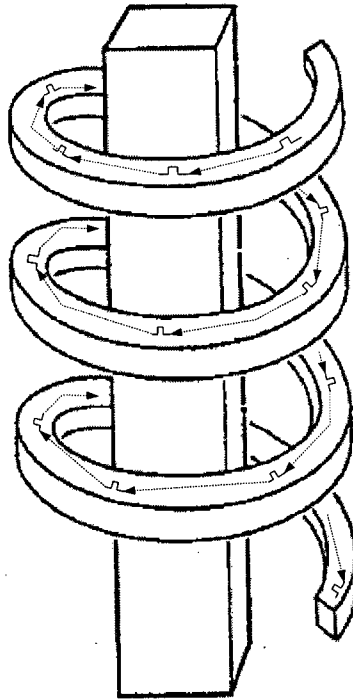
Figure 9: High frequency pulse traveling along transformer winding [12]

It is possible to conclude that at high frequencies the traveling wave model would be more suitable as a circuit representation of the winding. It follows that a signature based on the main parameter associated with the traveling wave can be used as a signature, namely the characteristic impedance, Z_c.

4.3 CHARACTERISTIC IMPEDANCE

An incremental length of line dx can be represented as shown in Figure 10.
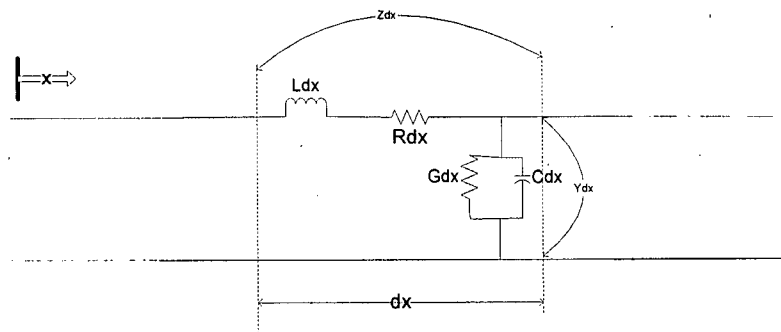
Figure 10: Incremental length of line

27

The incremental series impedance, Z and the incremental shunt admittance, Y are defined as:

$$Z = R_{dx} + j\omega L_{dx} \qquad (1)$$

$$Y = G_{dx} + j\omega C_{dx} \qquad (2)$$

From the circuit equations a set of differential equations is developed and the system can be expressed as the wave equations:

$$-\frac{dV}{dx} = ZI \qquad (3)$$

$$-\frac{dI}{dx} = YV \qquad (4)$$

Where V and I are phasors

The general solution for this system of equations is given by:

$$V = K_1 e^{-\gamma x} + K_2 e^{\gamma x} \qquad \text{Where } \gamma = \sqrt{Z.Y}$$

Substituting this back in the original equation:

$$V = \frac{K_1}{Z_c} e^{-\gamma x} - \frac{K_2}{Z_c} e^{\gamma x} \qquad \text{Where } Z_c = \sqrt{\frac{Z}{Y}}$$

$$Z_c = \sqrt{\frac{R(\omega) + j\omega L(\omega)}{G(\omega) + j\omega C(\omega)}} \qquad (5)$$

At sufficiently high frequencies, due to skin effect (discussed in the next section), the frequency dependent resistance can be modeled as $R\sqrt{\omega}$. Also, for practical considerations the shunt conductance is negligible. Equation 5 reduces to:

$$Z_c = \sqrt{\frac{R\sqrt{\omega} + j\omega L(\omega)}{j\omega C(\omega)}} = \sqrt{\frac{R}{j\sqrt{\omega} C(\omega)} + \frac{L(\omega)}{C(\omega)}}$$

At very high frequencies current flows on the skin of the conductor alone, so that the inductance is completely external. Since the conductor is comprised of free moving charges there is no steady state electric field within the conductor so that the capacitance is due to external flux alone. The equation is reduced to the following at high frequencies:

$$Z_c = \sqrt{\frac{L(\omega)}{C(\omega)}} = \sqrt{\frac{L_{EXTERNAL}}{C_{EXTERNAL}}} \tag{6}$$

Which is constant

4.4 FREQUENCY DEPENDENCE (THE SKIN EFFECT)

Skin effect is the name given to the phenomenon whereby AC current tends to flow closer to the surface of a conductor as frequency is increased. This is due to the current being guided by a medium (copper) of a different permeability than the medium surrounding it (oil paper insulation). As a result the inductance of the conductor increases with depth. As frequency is increased the inductive reactance $j\omega L$ also increases resulting in higher impedance at the centre of the conductor which forces current to flow to the outside.

This affects the velocity of propagation because the velocity with which current wave propagates is related to the rate at which the electric and magnetic fields it generates can develop. This is dependent on the permittivity and the permeability of the medium in which the fields are generated. At low frequencies current still flows at a relatively large depth inside the conductor. This means that there are two media involved in propagation, the copper winding and the insulation around it. The wave speed is limited by the higher permittivity of the copper and so travels more slowly. As frequency increases, the current flows increasingly to the surface of the winding. A greater percentage of the fields are generated in the external medium. At very high frequencies, the current flows on the skin of the conductor. Approximately all of the fields are developed in the external insulating medium and consequently the wave is allowed to propagate at its fastest. The wave propagation speed is entirely independent of the geometry of the winding or the capacitance and inductance. However, it is related to the capacitance and inductance through the equation below (assuming very high frequency):

$$v = \sqrt{\frac{1}{\mu\varepsilon}} = \sqrt{\frac{1}{L_{EXTERNAL} C_{EXTERNAL}}} \tag{7}$$

29

v can be calculated from readily available values of μ and ε, thus if either the $C_{EXTERNAL}$ or $L_{EXTERNAL}$ is known the other can be calculated.

4.5 APPLICATION OF THEORY TO WINDING MOVEMENT

Effect of separation on Z_c

Consider first an unraveled winding, which can be represented as a transmission line
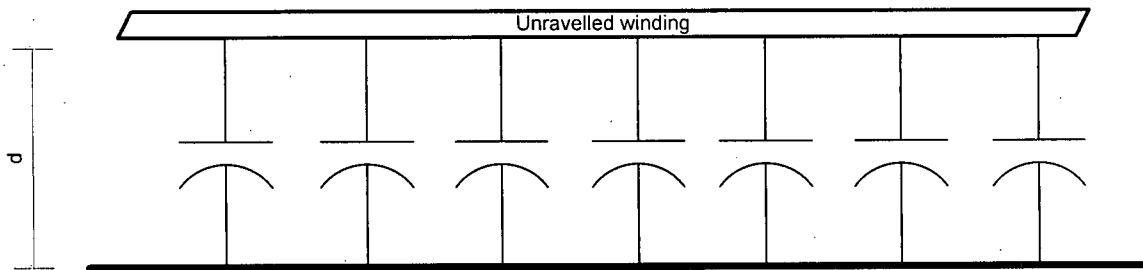
Figure 11: capacitance to ground for unraveled winding

The rectangular construction of the windings allows us to calculate the capacitance of the winding to ground by using the well known equation for parallel plate capacitors:

$$C = \frac{\varepsilon A}{d} \tag{8}$$

Since the cross sectional area per unit length remains the same as well as the permittivity of the insulation the only factor seen to influence the capacitance is the distance from one surface to another.

If the distance, 'd', changes, there is a corresponding change in the capacitance; the inductance is correspondingly scaled in the opposite direction, since the LC product must remain the same (the velocity remains constant). This scaling is reflected exactly in the characteristic impedance as the following equations illustrate:

30

$$WITH \quad Z_c = \sqrt{\frac{L_{EXTERNAL}}{C_{EXTERNAL}}} \qquad (9)$$

$$L_{EXTERNAL} = \frac{1}{v^2 C_{EXTERNAL}} \qquad (10)$$

$$THEN \quad Z_c = \sqrt{\frac{1}{v^2 C^2_{EXTERNAL}}}$$

$$Z_c = \sqrt{\frac{d^2}{v^2 \varepsilon^2 A^2}}$$

$$Z_c = d\sqrt{\frac{1}{v^2 \varepsilon^2 A^2}}$$

$$Z_c = d.K \qquad (11)$$

A change in the distance, d, is reflected by a proportional change in Z_c. The actual model is not this simple, however, since the winding is coiled as shown in Figure 12.
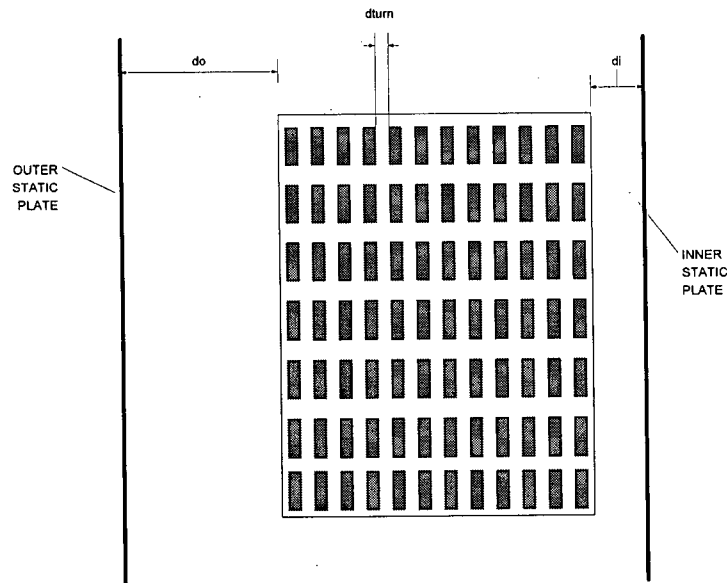
Figure 12: Winding between two static plates

The external capacitance is not due to a single source, e.g. capacitance to ground or capacitance. There are also capacitances between adjacent turns and between adjacent layers. As a result the simple relationship between the characteristic impedance and the capacitance may not hold true.

31

Derivation of measurement equations

The equations developed thus far deal with Z_c in terms of the circuit parameters L and C, for diagnostic purposes however these are not directly measurable. A method of calculating Z_c from measurable data is needed.

Traditionally, characteristic impedance measurements, such as those used to measure the characteristic impedance of co-axial cables, involve open and short circuit tests. The open and short circuit input impedances are measured and the characteristic impedance is found by the following equation:

$$Z_c = \sqrt{Z_{open} \times Z_{short}} \quad = \sqrt{\frac{R + j\omega L}{G + j\omega C}} \qquad (12)$$

The open circuit impedance is the inverse of the shunt admittance ($\frac{1}{G + j\omega C}$) and the short circuit impedance gives the series impedance $(R+j\omega L)$. This measurement method however, would require offline testing of the transformer. Since the eventual aim of the Transmission Line Diagnostic method is to have online measurements then a different method must be derived.

The equivalent circuit for the frequency dependent line as well as the derivation of the measurement equations are given on the following page:
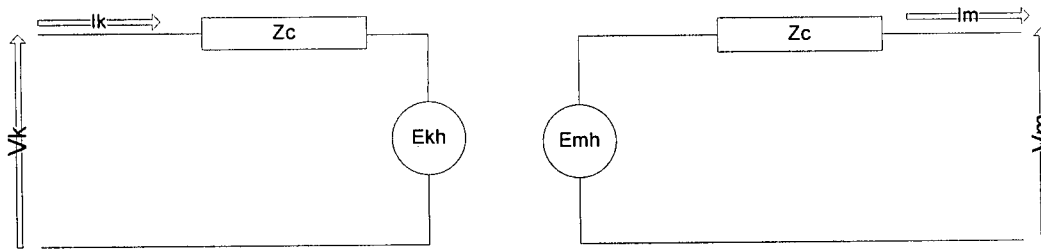
Figure 13: Equivalent Circuit for Frequency dependent line

$$E_{kh} = (V_m - Z_c I_m) \, e^{-\gamma l} \qquad (13)$$

$$E_{mh} = (V_k + Z_c I_k) \, e^{-\gamma l} \qquad (14)$$

Applying Kirchoff's voltage law

$$V_k e^{-\gamma l} + Z_c I_k e^{-\gamma l} = Z_c I_m + V_m \dots \qquad (15)$$

$$V_k - Z_c I_k = Z_c I_m e^{-\gamma l} + V_m e^{-\gamma l} \dots \qquad (16)$$

From (15)

$$e^{-\gamma l} = \frac{Z_c I_m + V_m}{V_k + Z_c I_k} \qquad (17)$$

Substituting for this in equation (16):

$$V_k - Z_c I_k = \frac{V_m + Z_c I_m}{V_k + Z_c I_k}\left(V_m - Z_c I_m\right)$$

By cross multiplication:

$$\left(V_k - Z_c I_k\right)\left(V_k + Z_c I_k\right) = \left(V_m + Z_c I_m\right)\left(V_m - Z_c I_m\right)$$

$$V_k^2 - Z_c^2 I_k^2 = V_m^2 - Z_c^2 I_m^2$$

$$Z_c = \sqrt{\frac{V_k^2 - V_m^2}{I_k^2 - I_m^2}} \qquad (18)$$

It can be seen that the value of the characteristic impedance is obtainable through a simple equation involving measurable voltages and currents. These variables are all phasors. The output voltage and current is measured across an output resistor and the input voltage and currents are measured at the transformer terminals. In practice a swept frequency approach is used because of the inherently higher signal to noise ratio it involves. For testing purposes, the mock transformer constructed in the Department's High Voltage Lab last year (see Figure 14) was used.
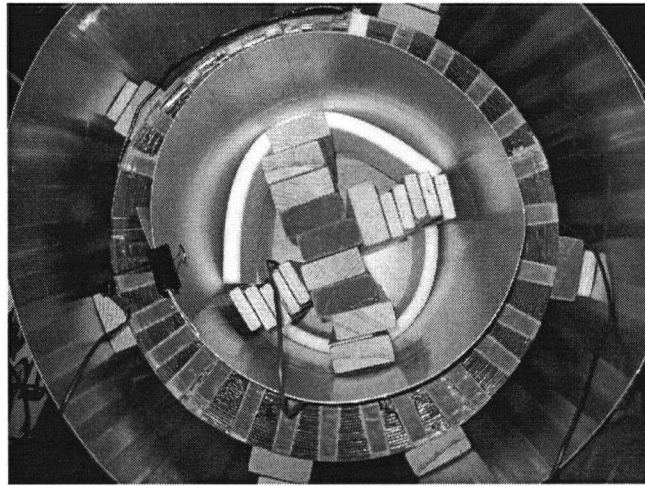
Figure 14: Mock Transformer at the HV Lab

This device facilitated a rough verification of the theory. However, since the method is sensitive to the construction of the transformer, the mock transformer is not ideal to test the effectiveness of the technique on large power transformers. Although some experiments were carried out at Powertech Labs, these so far could only verify that a signature of the expected form is obtained by measurement. Since simulating distortions could destroy a power transformer or for the least result in very high repair costs, it is necessary to develop a detailed transformer model that allows distortions to be simulated and the differences between signatures to be quantified.

CHAPTER 5: TRANSFORMER MODELLING

5.1 INTRODUCTION

The transformer is one of the most complex electrical elements in a substation. For power flow studies or even short circuit studies its complex nature is often trivialized as an inductance. However for the purpose of diagnostics, where the response of the windings is measured over a range of frequencies, such simplifications cannot be made.

Lumped (RLC) models are currently the most prevalent circuit models being used for studying the transfer functions of transformers. These models break the winding into sections containing as a series inductance and resistance with a lumped capacitance to ground as well as a lumped capacitance from section to section representing the inter-turn capacitance. It is not uncommon for windings to be split into as much as 60 or 70 sections for this type of model.

A model must be developed that is detailed enough to accurately depict the phenomena being simulated yet simple enough to allow simulation on available modern computing facilities. To determine how detailed the model should be, the physical layout of the transformer (particularly the winding arrangement) must be studied. In this section a useful Transmission Line model of the transformer is developed for diagnostic simulations. At this point it should be remembered that the characteristic impedance becomes constant and a quantifiable measure of winding displacement at high frequencies. The model developed will, therefore, focus on capacitive considerations.

5.2 THE MULTIPHASE MODEL

Figure 15 shows a typical arrangement for a disk type transformer.
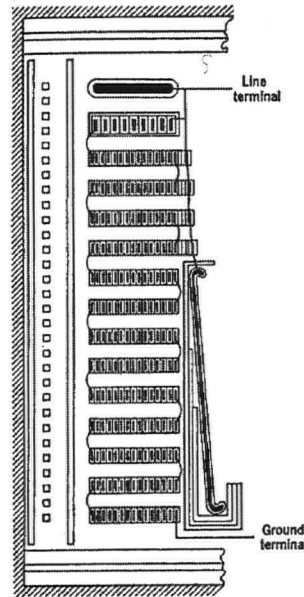
Figure 15: Cross section of winding arrangement in a disk type transformer [13]

Common assumptions used for the modeling of overhead transmission lines such as negligible proximity effect, uniform electric fields etc. can be called into question for the analysis of a transformer. In reality, there is capacitance from every surface on the inside of the transformer to every point of the winding. The distances between surfaces may vary, for example, the static shield is slanted, and corners of the tank are further from the windings than the centres of the tank walls. The close packing of the windings also brings in phenomena such as proximity effect.

Most of these irregularities, however, are negligible or can be averaged out without significant loss of accuracy. A cross section of the transformer such as the one shown in figure 15 reveals that, unlike a transmission line there is a capacitance from the winding to itself (due to coiling) corresponding to the capacitance between turns and the capacitance between layers. Since the turns and layers are coupled to eachother a single phase line cannot be used to represent the winding.

A more realistic approach is to use the multiphase line representation. The entire winding cross section as shown in Figure 15 would be viewed as a multiphase system, with each turn of each layer corresponding to a phase. The end of each phase is then connected to the start of the next phase to represent the winding as shown in Figure 16.
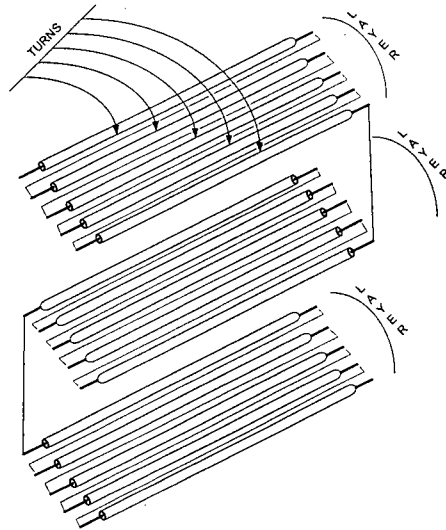
Figure 16: Multi-phase interconnection of windings

The transmission lines in the model use constant parameter (CP) representation. These lines are high frequency approximations to frequency dependent transmission lines. The parameters that need to be specified for these lines are the capacitance and inductance matrices. As discussed earlier, the process adopted is to estimate the capacitance based on winding construction and then calculate the inductance which is obtainable through the equation relating inductance, capacitance and velocity of propagation. Some considerations in modeling the capacitance of the windings are outlined in the following sub-sections.

Intra-turn capacitance

Capacitance arises from the electric field between a plane and any other surface that does not lie on that plane. For this reason there is no capacitance from one point of a horizontal transmission line to a point further down that line. In the case of transformers however, the winding is coiled so that there is capacitance between every point on a coil to every other point (see Figure 17).
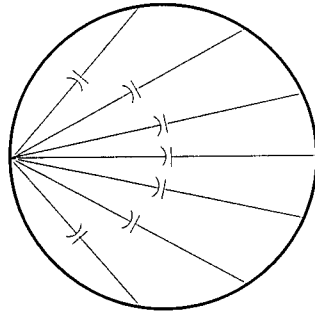
Figure 17: Intra turn capacitance for a single coil of the transformer

The capacitance of a transmission line to itself cannot be modeled. The model would, therefore, have to contain transmission lines of such a small size that they would be relatively straight, not curved. This would require an extraordinary amount of transmission lines to model even a single turn. However, the space between the turn is occupied by other turns or the core which in effect blocks the electric flux that would give rise to the intra turn capacitance. This means that the intra-turn capacitance is greatly reduced as shown in Figure 18.
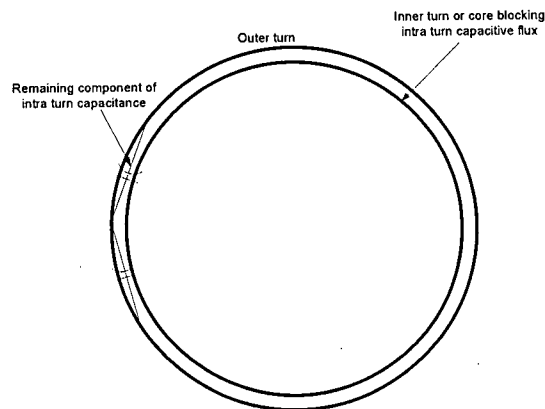
Figure 18: Inner turn or core blocking intra turn capacitance

From Figure 18 it can be seen that as the distance between the turns decreases the intra-turn capacitance also decreases. The only separation between the turns is the oil-impregnated paper (a relatively small distance), hence this capacitance can be neglected.

Capacitance from windings to external surfaces

A basic assumption made is that the capacitance to any surface is due to a uniform electric field, that is, both surfaces form a parallel plate capacitor, the area of which is set to the area of the winding surface involved, (see figure 19 and 20).
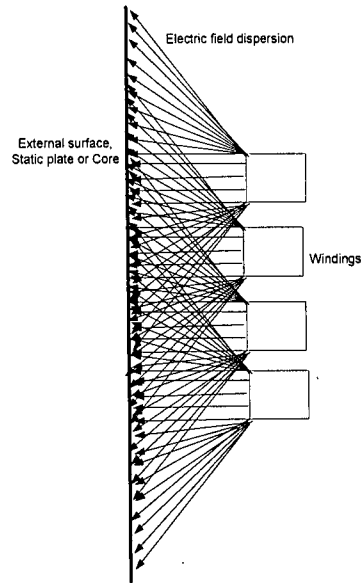
Figure 19: Actual electric field between windings and external surface
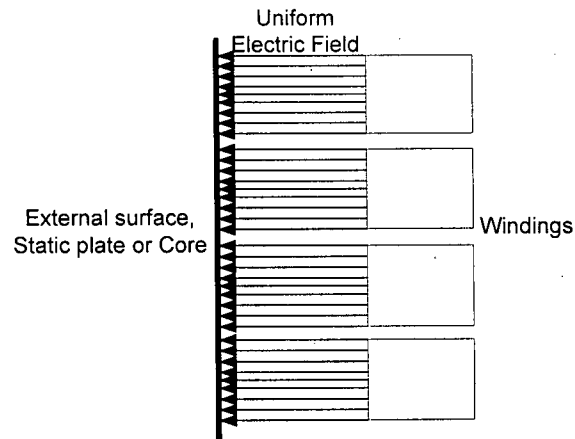
Figure 20: Approximated electric field between windings and external surface

This is not at all a poor assumption since the edge effects of adjacent windings interact to produce a net flux perpendicular to the winding and external surfaces. Only the edge effects of the top and bottom windings would not have this interaction. However, considering total height of the winding structure then these can be ignored.

Inter-turn capacitance

The capacitance between turns is treated in a similar way to capacitance from the turns to external surfaces in that the edge effects are neglected. The electric fields that are assumed present are those directly above, below and directly to the side of a turn. Figure 21 shows the electric field distribution considered. The dotted lines are examples of fluxes that would be ignored.
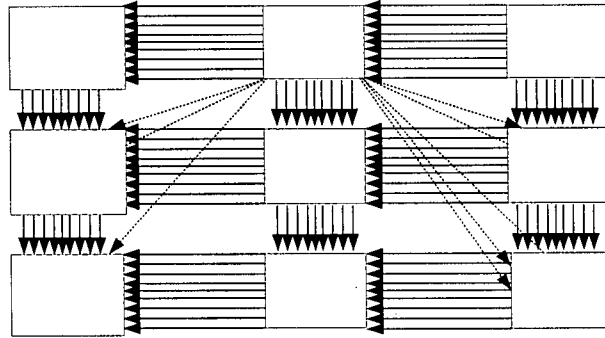
Figure 21: Electric field assumed between windings

Apart from these two assumptions of uniformity, the only other assumption with respect to the modeling of the capacitance is its dependence on location of the turn in the winding structure. Since capacitance is dependent on the electric field, turns at different locations of the windings would experience different net electric fields. For example the turn on the top left corner of Figure 21 has only capacitance to two turns while the one at the centre has capacitance to 4 turns. To model this, the winding was separated into 9 main sections as illustrated in Figure 22.
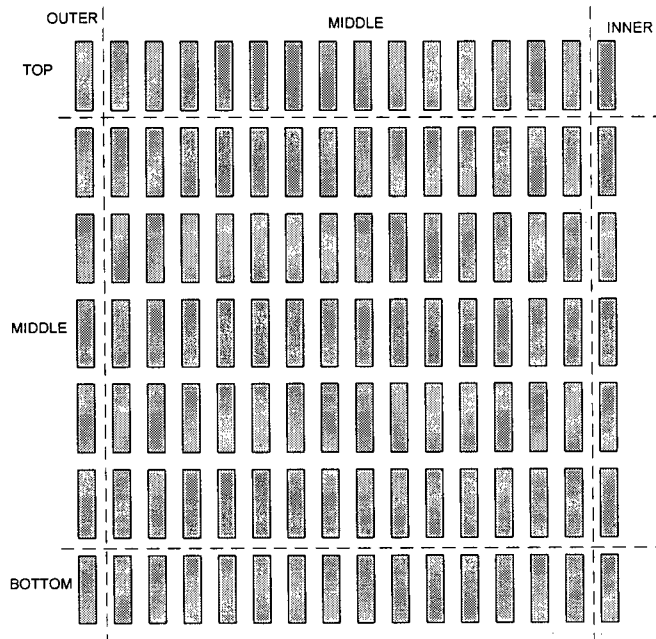
Figure 22: Separation of winding for capacitance distribution

The capacitance for each of the nine sections can be separately specified. This allows the user to determine whether the capacitances (to ground for instance) should be distributed equally throughout the length of the winding or should it be confined to a particular set of windings alone.

Modeling of Resistance

Although both the inductance and the resistance are dependent on the skin effect the inductance is taken to be constant at the value of the external inductance while the resistance is altered at every simulated frequency.

Two options are provided for the calculating of the resistance. The first is simply an application of Lord Rayleigh's observation that at sufficiently high frequencies the resistance is proportional to the square root of the applied frequency

$$R \propto \sqrt{f}$$

Though this is traditionally applied to overhead cables that have circular construction it can also be shown to be true for conductors of rectangular construction. Consider the

rectangular section of dimensions x and y below through in which current is flowing through the shaded region:
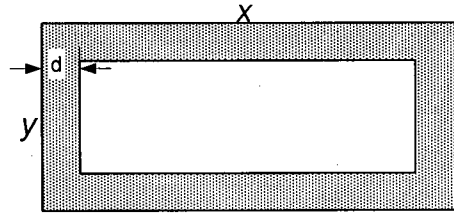
Figure 23: Skin effect due to high frequency, current only flows through shaded region

$$A_{DC} = xy$$
$$A_{hf} = xy - (x - 2d)(y - 2d)$$
$$A_{hf} = 2xd + 2yd + 4d^2$$

$$R = \frac{\rho l}{A} = \frac{\rho l}{2xd + 2yd + 4d^2} \qquad (19)$$

$$where \quad d = skin\, depth = \sqrt{\frac{1}{\mu \pi f \sigma}} = \frac{k}{\sqrt{f}} \qquad (20)$$

$$R = \frac{\rho l}{2x\frac{k}{\sqrt{f}} + 2y\frac{k}{\sqrt{f}} + 4\frac{k^2}{f}}$$

$$as\ f \to \infty\, f : R = \frac{\rho l}{\frac{k}{\sqrt{f}}(2x + 2y)}$$

$$R = K\sqrt{f} \qquad (21)$$

$$where\, K = \frac{\rho l}{k(2x + 2y)}$$

42

Using this method the resistance of the winding at a known high frequency is entered; the value of the constant K is calculated and used to recalculate the resistance at every new frequency.

The second option allows the user to enter the conductor dimensions, the conductivity and permeability of the rectangular conductor. Using the conductivity and permeability the skin depth at a particular frequency is calculated, the resistance is then calculated by using the area through which current flows and the resistivity of the conductor. This method is expected to be more accurate for lower frequency simulations where the high frequency approximations made do not hold. For the general application of this model proposed (high frequencies) both methods should give roughly the same results.

By either method the resistance calculated is the resistance corresponding to the length of the winding section used and is placed in series with winding section.

5.3 PROGRAM STRUCTURE

The software was developed in the MATLAB v7.04 programming environment for data processing while the Microtran Circuit Simulator (an external program), was used for carrying out simulations. The entire simulation process involved four main stages sequentially run in the order below:

1. Calculation of parameters.
2. Data file generation.
3. Running Simulations.
4. Processing output files.

The process is now completely automated and does not require Microtran to be run separately by the user as was the case in earlier software iterations. The following sub-sections outline the main responsibilities of each stage of the simulation process.

Calculation of parameters

The program requires the user to input the following data regarding the transformer winding to be tested:

- Number of turns per pancake.
- Number of pancakes.
- Turn length.
- Inter pancake capacitance.
- Inter turn capacitance.
- Capacitance to ground.
- Capacitance to static plates.
- Velocity of propagation.
- Transformer MVA.
- Transformer kVA.
- Resistance at a specified high frequency.
- Amplitude of signal.
- Vector of frequencies to be simulated.

The number of turns per pancake, number of pancakes and the capacitances specified are used to generate the capacitance matrix which is of the following form for a system with *5* turns and *2* pancakes.

$$
\left[
\begin{array}{ccccc|ccccc}
\sum C_{ext_{11}} & -C_{it} & 0 & \cdots & 0 & -C_{ip} & & & & 0 \\
-C_{it} & \sum C_{ext_{12}} & -C_{it} & 0 & \vdots & & -C_{ip} & & & \\
0 & -C_{it} & \sum C_{ext_{13}} & -C_{it} & 0 & & & -C_{ip} & & \\
\vdots & 0 & -C_{it} & \sum C_{ext_{14}} & -C_{it} & & & & -C_{ip} & \\
0 & \cdots & 0 & -C_{it} & \sum C_{ext_{15}} & 0 & & & & -C_{ip} \\
\hline
-C_{ip} & & & & 0 & \sum C_{ext_{21}} & -C_{it} & 0 & \cdots & 0 \\
 & -C_{ip} & & & & -C_{it} & \sum C_{ext_{22}} & -C_{it} & 0 & \vdots \\
 & & -C_{ip} & & & 0 & -C_{it} & \sum C_{ext_{23}} & -C_{it} & 0 \\
 & & & -C_{ip} & & \vdots & 0 & -C_{it} & \sum C_{ext_{24}} & -C_{it} \\
0 & & & & -C_{ip} & 0 & \cdots & 0 & -C_{it} & \sum C_{ext_{25}}
\end{array}
\right]
$$

Figure 24: Illustration of phase capacitance matrix for 2 pancakes with 5 turns each

The number of matrices on the diagonal is equal to the number of pancakes and the size of each of these matrices corresponds to the number of turns. The following points should be noted:

- The inter pancake couplings form the diagonal elements of the off diagonal matrices.

- There is no inter-turn capacitance C_{it} in the off diagonal matrices

- The Diagonal elements are the sum of all included capacitances including the inter turn; inter pancake and ground capacitances.

- The off diagonal elements, namely C_{ip} and C_{it} are fixed while the sums calculated for the diagonal elements can be changed according to the position of the winding (outer-top, middle-top etc).

Once this matrix is obtained, it is used to calculate the inductance matrix using the equation relating capacitance inductance and velocity:

$$[L_{EXTERNAL}] = \frac{1}{v^2}[C_{EXTERNAL}]^{-1} \qquad (22)$$

The capacitance matrix is then diagonalized by a similarity transformation. It should be noted that the same matrix that diagonalizes the capacitance matrix also diagonalizes the inductance matrix.

Data file generation

The transformer includes a number of large multiphase systems that need to be simulated at a number of frequencies so the data files become exceedingly long, approximately 1500 lines, and therefore cannot be written by hand. The data file format for Microtran is reproduced in Figure 25.

Item	Description
[1]	CASE IDENTIFICATION CARD.
[2]	TIME CARD.
[3]	LINEAR AND TRUE NONLINEAR BRANCHES.
$	Blank line to terminate section [3].
[4]	SWITCHES AND PIECEWISE LINEAR BRANCHES.
$	Blank line to terminate section [4].
[5]	SOURCES.
$	Blank line to terminate section [5].
[6]	USER-SUPPLIED INITIAL CONDITIONS.
[7]	NODE VOLTAGES OUTPUT.
[8]	POINT-BY-POINT USER-DEFINED SOURCES.
$	Blank line to terminate the data case.
	...... NEXT DATA CASE ....
$	Blank line to terminate the set of cases.

Figure 25: Data file format, reproduced from the Microtran product manual [14]

The data file is a text file that is read by columns. Node names were pre assigned based on the layer and turn of the winding as shown in Figure 26.
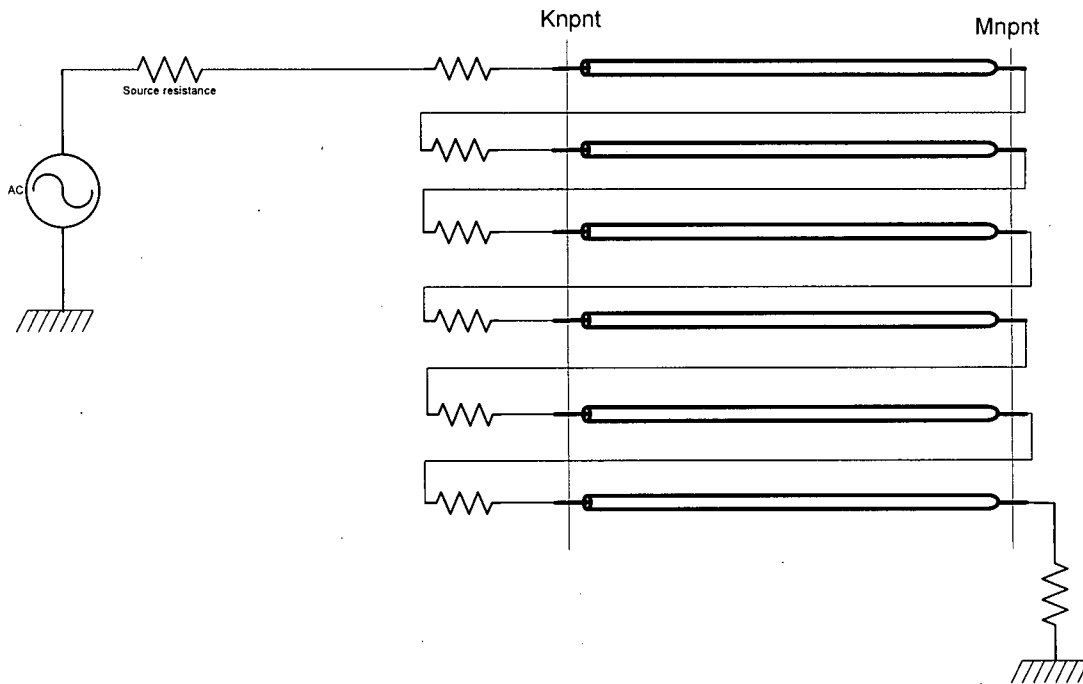
Figure 26: Circuit set up for Microtran simulations

In the above circuit the nodes on the sending end of the transmission line are named 'k' followed by the pancake number 'np' and then the turn number 'nt' which it represents. The receiving end is named 'm' followed by 'np' and 'nt' for the pancake and turn which it represents. The lumped resistance represents losses and the lumped inductance is the propagation leakage. The details of the data card formats are available in the Microtran Reference manual and shall not be reproduced here.

The root name of the data case is specified by the user, e.g. 'base_case' and the program generates a sequence of cases bearing this name for each frequency in the vector of frequencies specified. For example if five frequencies are specified the program will generate the following files:

base_case1.dat

base_case2.dat

base_case3.dat

base_case4.dat

base_case5.dat

Running simulations

Running Microtran has been automated in two ways in the Matlab program. The first method entails saving all the generated data files into the same folder as the Microtran executable programme. All "*.dat" files should be configured to open with the Microtran executable. The "winopen" function in Matlab is then used to open the file.

The second method uses the command prompt to run Microtran and does not require files being placed in special folders or being configured to open using the Microtran executable. In this method the dos prompt was used to open Microtran from Matlab, passing it the name of a the simulation file for microtran to run. The output file is in the same directory of the input file specified.

Processing output files

Once the output files have been generated, the program can search for these files which have the same names as the input files e.g.

base_case1.out

base_case2.out

base_case3.out

base_case4.out

base_case5.out

The output data from Microtran is formatted. By counting a predetermined number of spaces from the end of the file the voltage and current output data can be extracted. This is done for each file and a value of characteristic impedance, trans-admittance and trans-impedance are calculated. When all the files are read the points are automatically plotted along with the numerical differences and the percentage difference between the plots (if two plots are specified).

The following chart summarizes the entire program
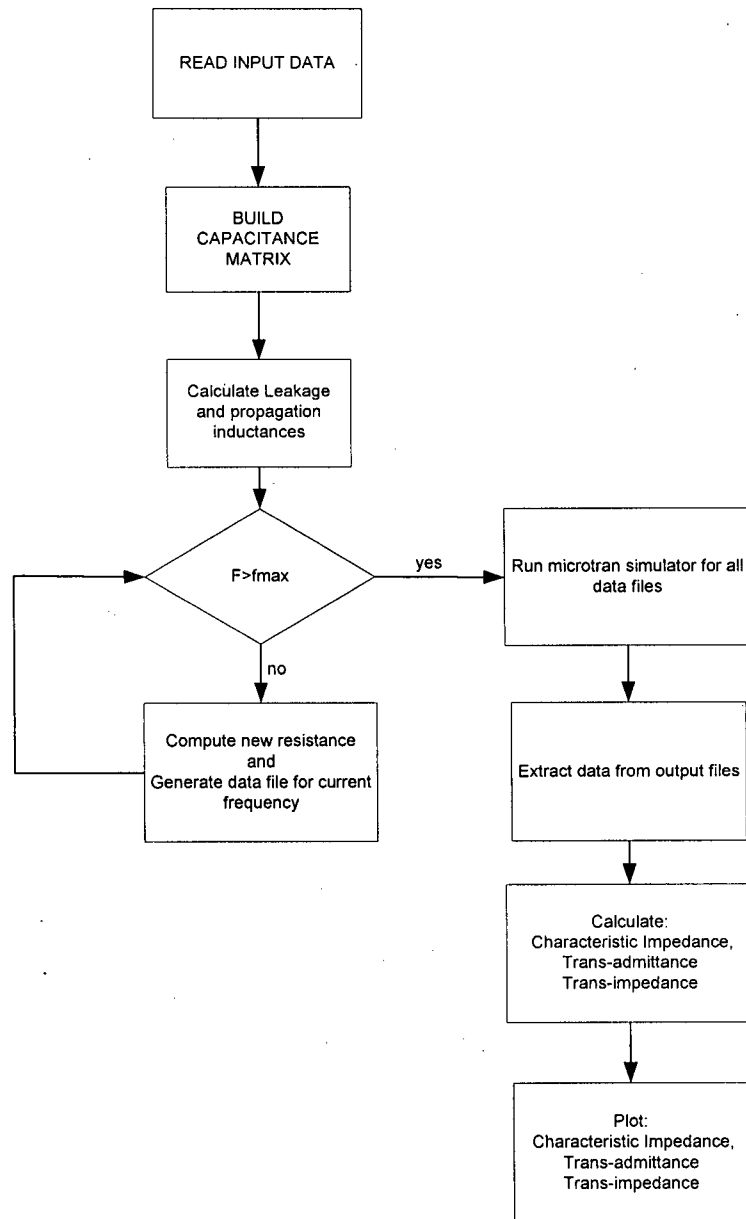
Figure 27: Algorithm for developed software

CHAPTER 6: MEASUREMENT AND MODELLING ISSUES

6.1 INTRODUCTION

This section explores the influence of the frequencies at which measurements are taken, the influence of lumping elements and phase error. The data for the transformer simulated is given in Table 6.

	Value	Units
Number of turns	20	
Number of pancakes/layers	12	
Length of turn	10	metres
Inter-pancake capacitance	27.28	pF
Inter-turn capacitance	158	pFm^{-1}
Surge velocity	200x10^6	ms^{-1}
Power rating	900	MVA
Voltage rating	525	kV
Input resistance	150	Ohms
Output resistance	1	Ohms

Table 6 : Data for simulated transformer

6.2 EFFECT OF FREQUENCY ON MEASUREMENT

The frequencies at which characteristic impedance measurements are taken can affect the accuracy of the results. To illustrate this a simple test was done (the test set up is shown in figure 28).
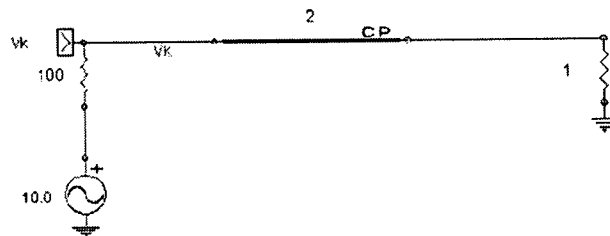
Figure 28: Simple test set up to explore the effect of lumping, Zc=200, v=200x10^{6}ms^{-1}

RESISTANCE	$|Z_c|$ @25kHz	$|Z_c|$ @5kHz	$|Z_c|$ @75kHz
0 (IDEAL PROPAGATION)	200	0	200
1x10⁻⁶	200	52.3634	200
1x10⁻⁵	200	1.29E+05	200
1x10⁻³	200	1.31E+04	200
1	200	228.0056	200
10	200.2049	199.4332	200.0244
50	204.8852	201.2167	200.5597
100	217.7542	204.8939	202.2181
500	365.3291	274.2021	241.4978

Table 7: Results of simulation with different value of resistances at three important frequencies for fully distributed resistance

Table 7 shows that for the ideal case, frequencies of 25 kHz and 75 kHz produce accurate results while at 50 kHz the value is 0. Figure 29 shows the relationship between Z_c and the phase shifts between the input and output currents for some key frequencies.
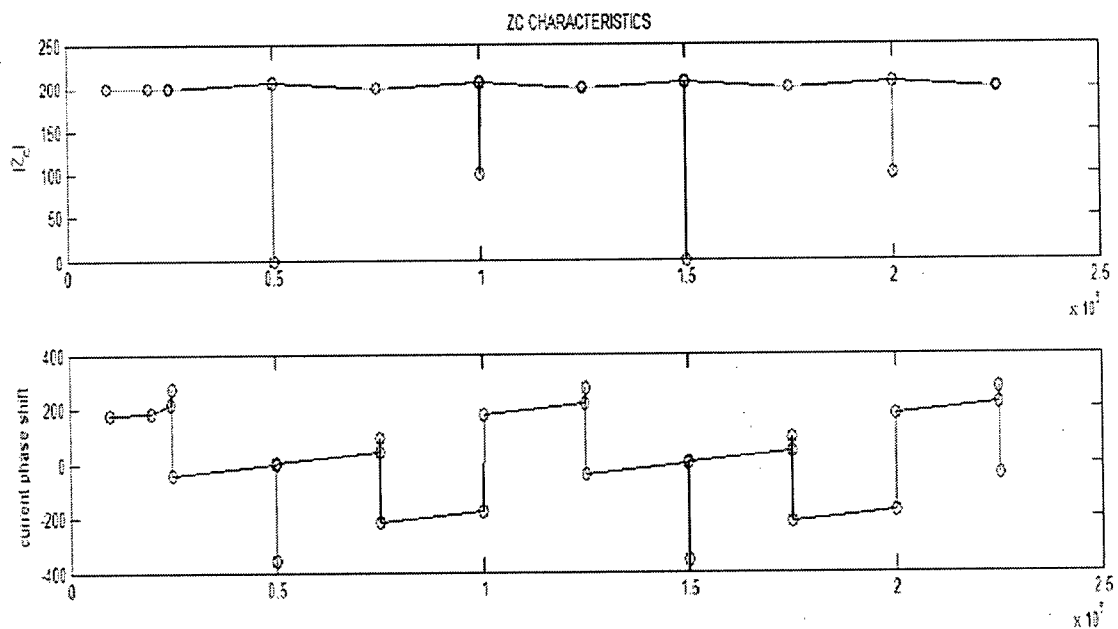
Figure 29: Relationship between Zc magnitude and phase shift between input and output currents for lossless line (R=0).

From figure 29 it can be seen that when the input and output currents are completely in phase (0°) or completely out of phase (180°) the results are erroneous (since there is no resistance the CP line should have a perfectly horizontal characteristic). The plots

51

suggest that there is an element of periodicity affecting the results. Errors of similar types occur at 50 kHz and 150kHz and 100 kHz and 200 kHz. This interval of 100 kHz corresponds to the characteristic frequency of the line.

This behaviour is due to standing waves being produced. When the input signal is periodic the delay corresponds to a phase shift and at multiples of the characteristic frequency the receiving end of the line falls in phase with the sending end of the line. Since there has been no loss over the length of the line the voltage and current waveforms at the receiving end are indistinguishable from the voltage and currents at the sending end. These frequencies in effect make the line look like a node. The measurement equation then becomes undefined since $V_k = V_m$ and $I_k = I_m$ yielding $Zc = 0/0$. This phenomenon is noticeable even for sizeable values of resistance such as 10Ω as can be seen from Table 6.

When the resistance increases to over fifty ohms, however, the results for 50 kHz begin to look more accurate. This is due to the fact that the output parameters have significantly smaller magnitudes because of the high losses. When the output falls in phase with the input they are not equal magnitude so that the numerator of the measurement equation (18) does not go to zero.

6.3 EFFECT OF LUMPING RESISTANCE

Transient simulations are needed for impulse testing. Due to restrictions in Microtran regarding the size of the specified resistance compared to the size of the characteristic impedance of a line (R/4 < Zc/10) it was not possible to add the resistances directly into the transmission line element. These had to be added externally in series to the transmission line elements.

To explore the effect of lumping on the model, consider the following four cases: a transmission line with a distributed resistance of 1000Ω ($2km = 1000\Omega$); 1000Ω lumped at the sending end of the line (Figure 30); 1000Ω lumped at the receiving end of the line

(Figure 31); and the resistance split equally between the sending and receiving end (Figure 32).

The frequencies chosen were the quarter, half and three-quarter frequencies of the characteristic frequency of the line (velocity/line length). These were specifically chosen because the lossless transmission line corresponds to a pure delay.
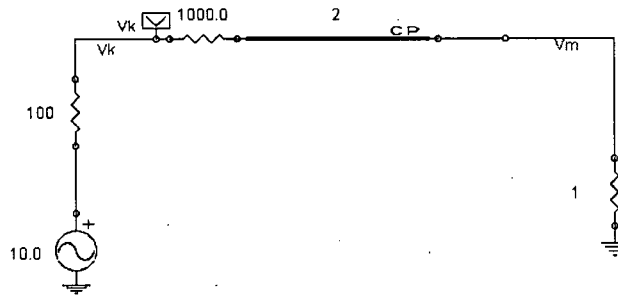
Figure 30: Resistance lumped at sending end of line
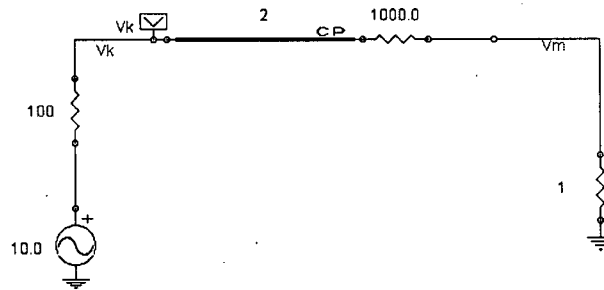
Figure 31: Resistance lumped at receiving of line
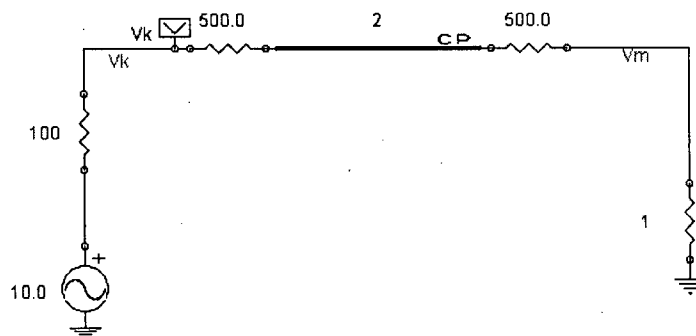
Figure 32: Resistance split between sending and receiving end of line

53

Location	Z_c at 25kHz / ohms	Z_c at 50kHz / ohms	Z_c at 75kHz / ohms
Distributed	*365.3291*	*274.2021*	*249.4978*
Front	205.0015	3.0307e+003	205.0015
Back	39.1868	18.2793	39.1868
Back and Front	538.5236	500.6786	538.5236

Table 8: Differences arising out of different lumped models.

Table 8 shows that the results for the distributed line are the most accurate. It shows a general decreasing trend with increasing frequency as expected. The lumped models however give oscillating results (first decreasing and then increasing or vice versa). It is therefore necessary to have as little lumping as possible for accurate simulation.

6.4 PHASE 'ERROR'
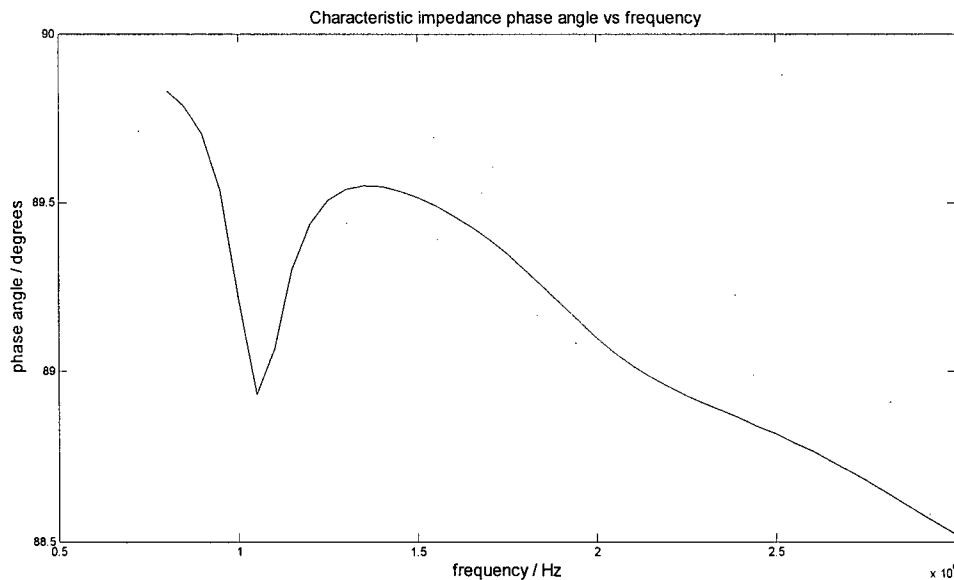
Figure 33: Variation of characteristic impedance phase angle with frequency

Figure 33 shows that the phase angle is in the region of 88 to 90 degrees when at high frequencies the angle should be approximately 0 degrees. This error is only seen in the multiphase model. This indicates that the inter turn capacitances may act as leakages that

54

provide alternate signal paths to the main path along the winding thus introducing phase shift.

It may also be due to the steady state measurement of the voltages and currents and the equation used to calculate the characteristic impedance (18). At high frequencies the multiphase transformer looks like a capacitive network. In steady state, therefore, the current leads the voltage by 90 degrees (verified from data). This is in turn reflected in the Characteristic impedance value as calculated by equation 18.

The large trough at 1MHz is an illustration of the error introduced by measurements at frequencies around the characteristic frequency. In this case, it is the characteristic frequency not of the entire winding or an individual turn but of a multiphase section (pancake, 200m).

CHAPTER 7: COMPARISON OF TLD AND FRA METHODS

7.1 INTRODUCTION

In this section the transformer model developed is used to simulate different types of fault conditions. Changes obtained from the Characteristic Impedance and trans-admittance signatures are also compared. The program developed also computes the trans-impedance signature which is simply the inverse of the trans-admittance signature. Those plots, however, are not reproduced in the main body of this report as its strengths and shortcomings are the same as those of the trans-admittance. Simulations are performed up to frequencies of 3MHz which is higher than the limit of 2MHz used in the physical experiments performed at Power Tech Labs.

The winding deformations simulated are divided into four main categories

1. Changes in line resistance
2. Winding bulging
3. Winding loosening
4. Winding compression

7.2 EFFECT OF WINDING RESISTANCE

The basic simulations have shown lumping to be critical to obtaining good results. The multiphase model uses 240 sections of line, this means the external line resistance is somewhat, though not fully, distributed. The code was amended to fully distribute the resistance using the exact pi-circuits in steady state solution. The line resistances were specified as a percentage of Z_{base}. For the purpose of simulations the percentage was varied between 1% and 200%. Although resistances above of 10% of Z_{base} may never be seen in reality they are simulated for the sake of illustration.
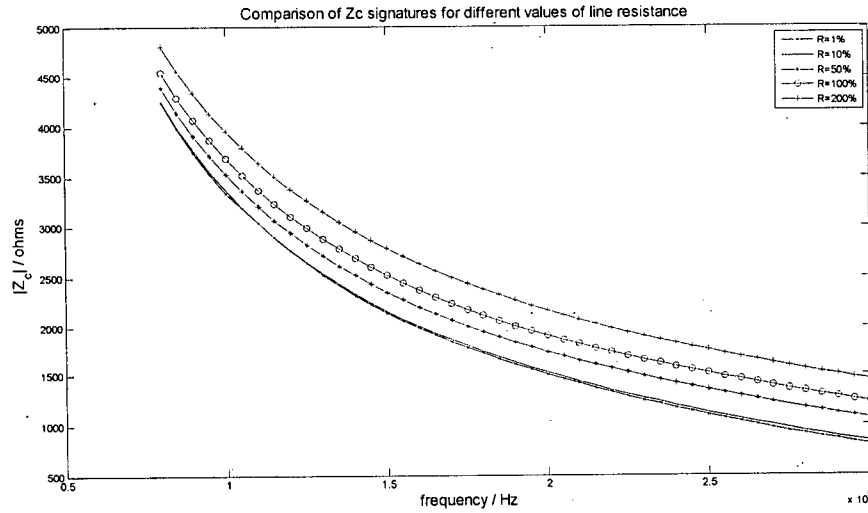
Figure 34: Z_c different values of input resistors

Figure 34 shows that as the resistance increases there is a corresponding upward shift of the characteristic impedance.
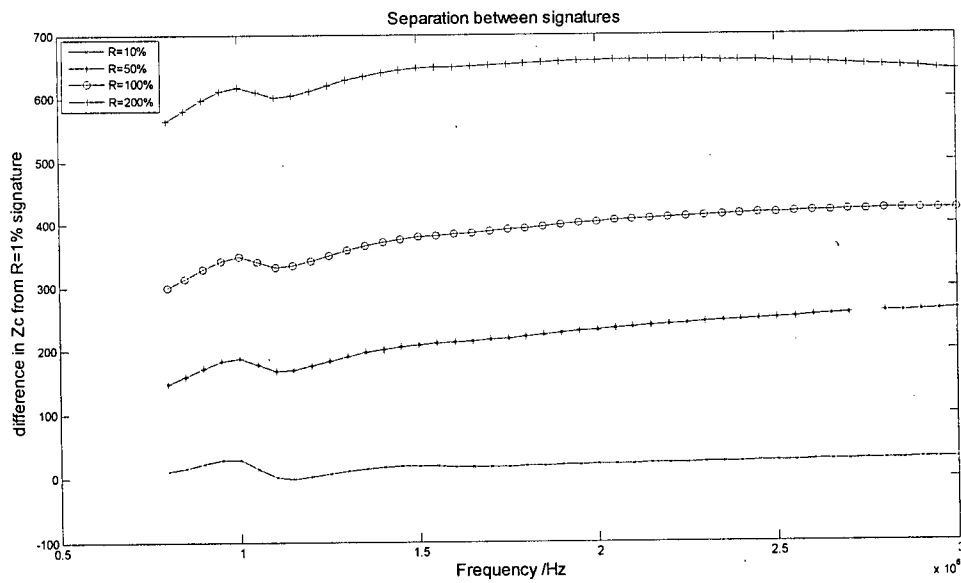
Figure 35 : Relatively constant separation between signatures

Figure 35 shows the separation between the signatures. Except for the initial slight oscillation the separation between the curves remains relatively constant.
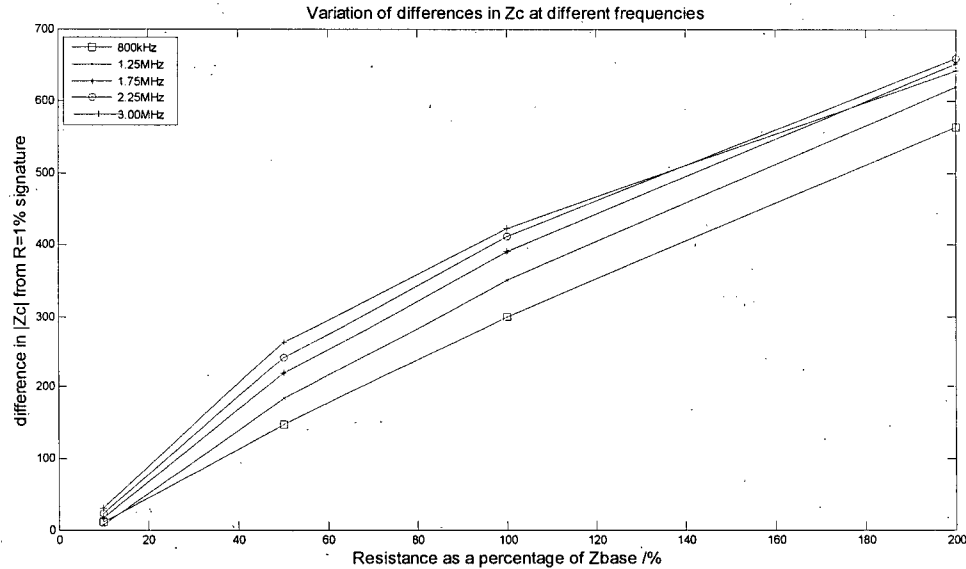
Figure 36: Change in Z_c for different winding resistances at different frequencies

Figure 36 shows that the percentage change in Zc with the percentage change in resistance is almost linear. The separation between the plots is due to the fact that the separations are not exactly constant over the frequency range. As the frequency increases the separation between the signatures (Figure 34) also increases slightly. It should be noted however that the higher frequency plots of Figure 36 seem to be closer together. This is because at higher frequencies the signatures level off. It would be better, therefore, to use higher frequency measurements in any attempt to quantify the winding movement from the plots.
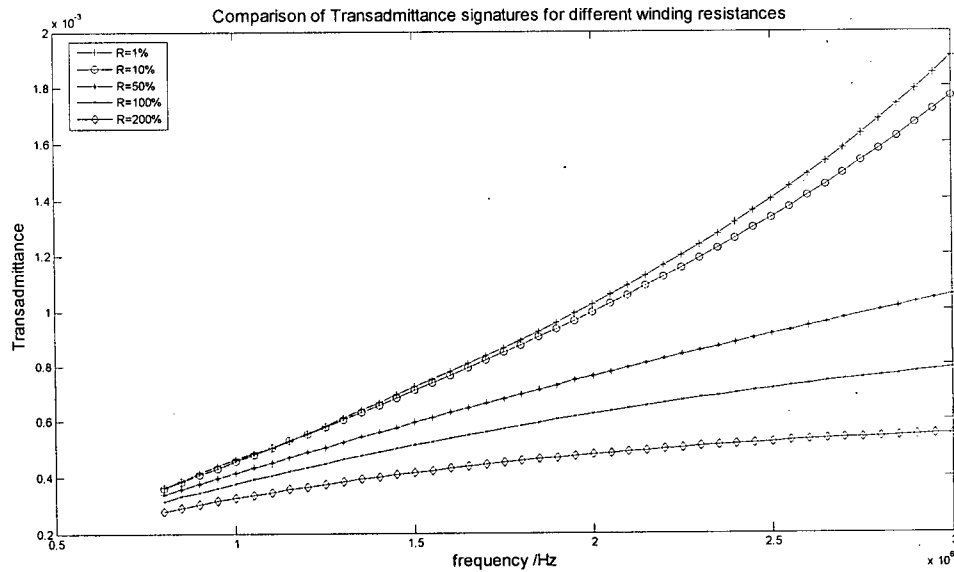
Figure 37: Transadmittance characteristics for different values of input resistors

Figure 37 shows the transadmittance signatures for the same cases as Figure 33. The separation between the curves varies considerably with frequency, unlike the case of the characteristic impedance. Figure 38 shows the differences of the plots at different frequencies.
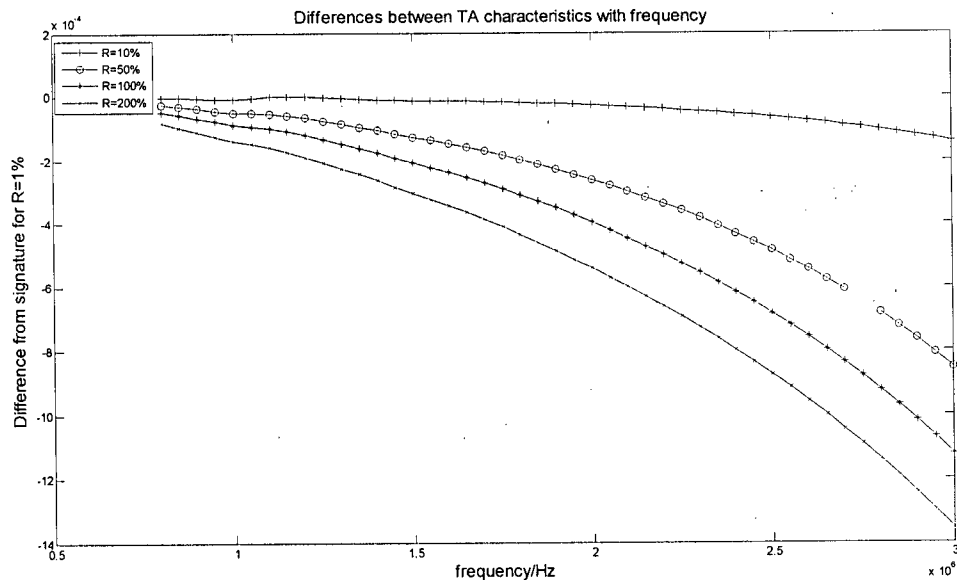
Figure 38: Separation between characteristics from R=1% signature

Figure 39: Change in TA for different winding resistances at different frequencies

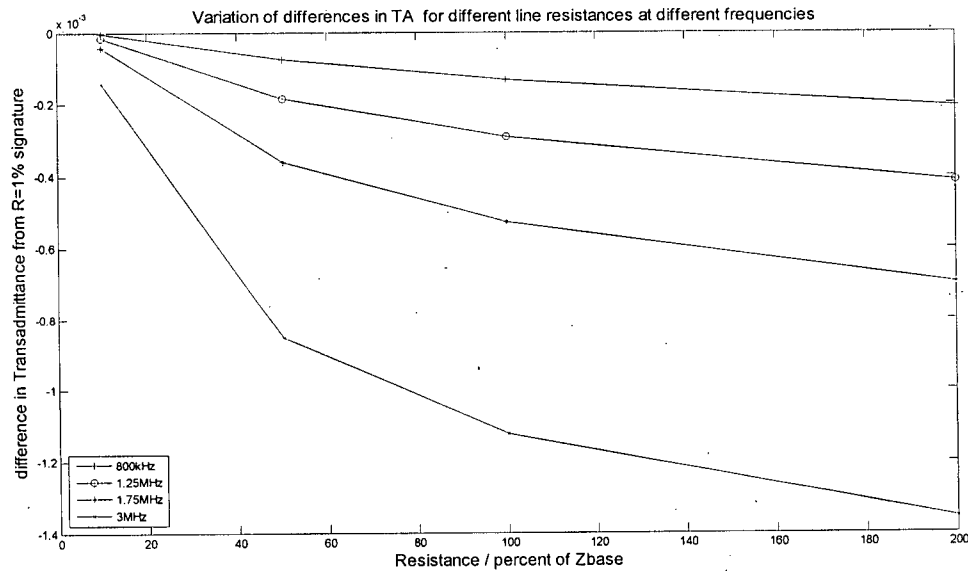Figure 39 shows that specific frequencies cannot be chosen to analyze the differences between the transadmittance plots as can be done for the characteristic impedance. Transadmittance characteristics are not monotonically decreasing functions like the characteristic impedance, but contain resonant peaks. The frequency range used for simulation does not show any resonant peaks, however, figure 37 shows that the plots for low values of line resistance seem to be bent upward, in the shape of the low frequency side of a resonant peak. The plots for higher values of resistance do not have this shape indicating that their resonant peaks may be at higher frequencies. These resonances make the interpretation of the Transadmittance signatures more complicated than the characteristic impedance signature.

7.3 WINDING BULGES

The winding bulge case is simulated by assuming that all the ground capacitance of the winding is to the tank. When the winding bulges, the windings come closer to the tank and so the ground capacitance increases. The parameter data borrowed for the model [15] did not specify distance to tank, so the capacitance is changed by percentage. Figure 4- shows the deviation of the Z_c signatures for 5%, 10%, 15% and 20% increases in the capacitance to ground.

Figure 40: $|Z_c|$ signatures for variations in C_g
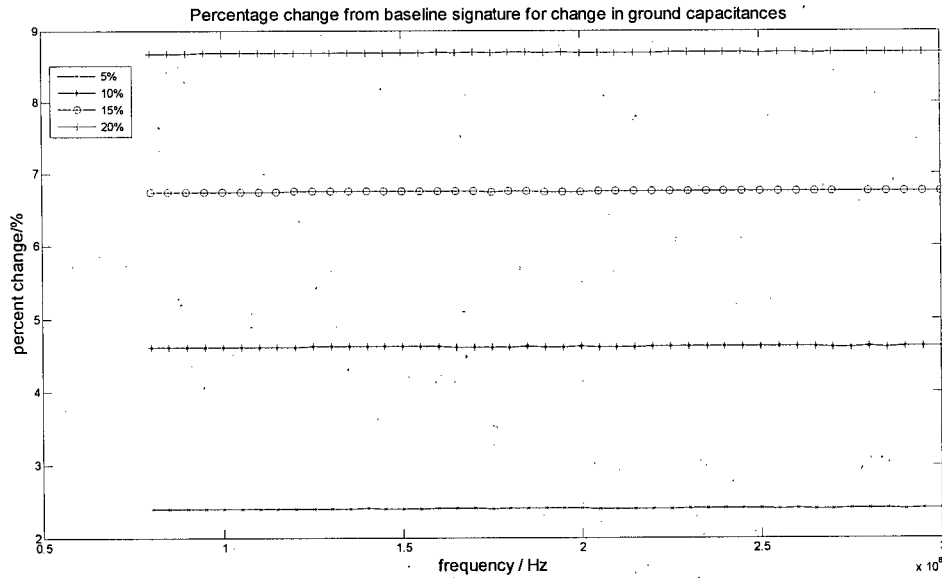
Figure 41: Percentage deviations from base plot for $|Z_c|$ for variation in C_g

Figure 41 shows that the percentage change between the plots remains relatively constant throughout the frequency range. The measured percentage changes are related to the actual change in capacitance through a simple scaling factor:

$$Actual\ change = Measured\ change \times K$$

61

Actual percent Change /%	Measured percent change /%	Scaling factor (K)
5	2.3971	2.0858
10	4.6192	2.1649
15	6.7433	2.2244
20	8.6879	2.3021

Table 9: Actual and measured percentage changes for Z_c signature for winding bulges

Table 9 shows that the scaling factor remains relatively constant (10% change from smallest to largest). This indicates that the measured percentage change can be used to directly estimate the physical bulge of the winding if the scaling factor can be determined.
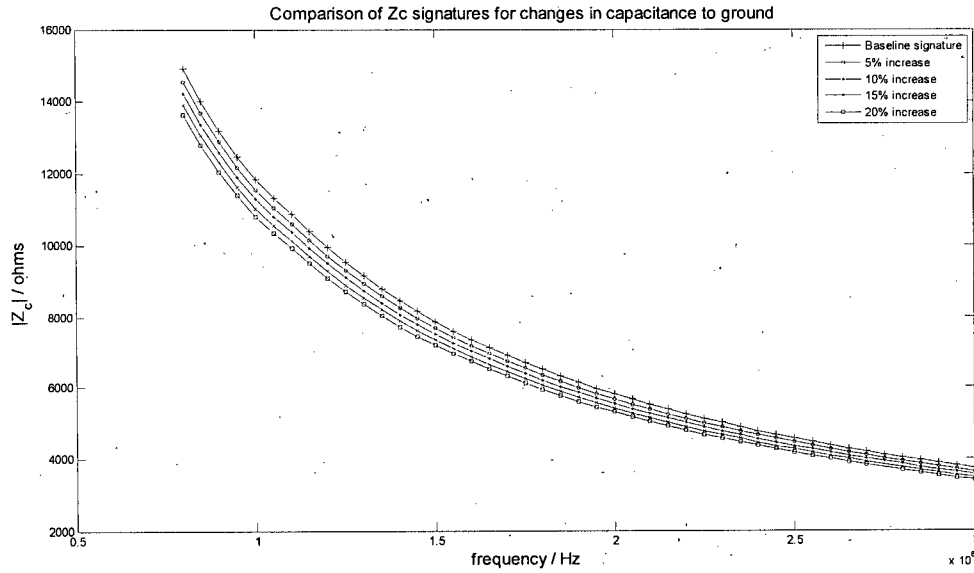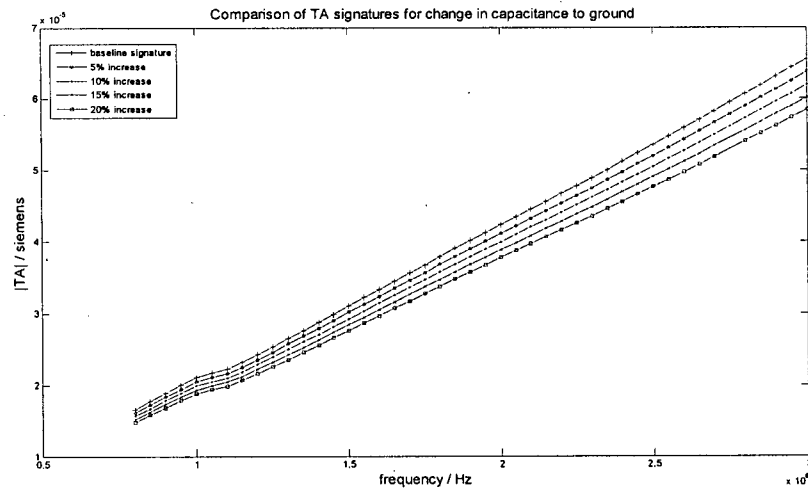

Figure 42: |TA| signatures for variations in C_g
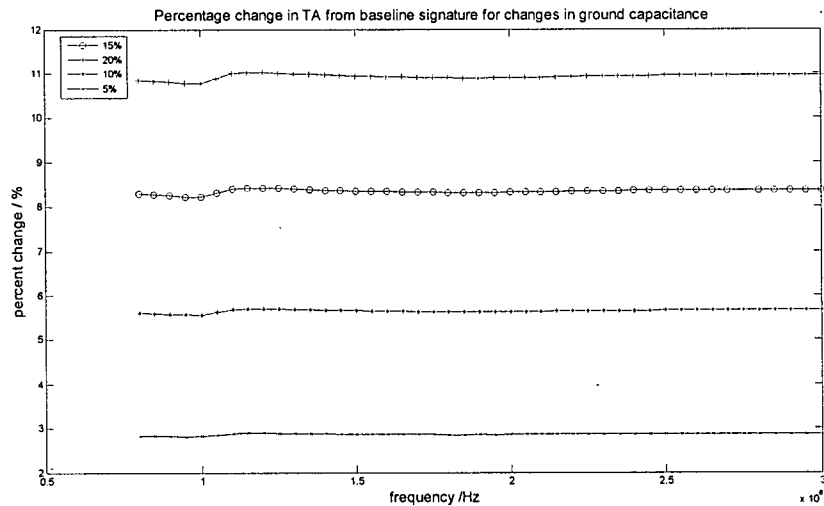
Figure 43: Percentage deviations from base plot for |TA| for variation in C_g

62

Actual percent Change /%	Measured percent change /%	Scaling factor (K)
5	2.8597	1.7484
10	5.6444	1.7717
15	8.3345	1.7997
20	10.9169	1.8320

Table 10: Actual and measured percentage changes for TA signature for winding bulges

Figure 43 and table 10 show that the transadmittance signatures exhibit similar behaviour to the characteristic impedance signatures in that the percentage change in the signatures are relatively constant. This however can only be said because no resonances have been encountered. The change in characteristic has the effect not only of changing the magnitude of the resonant points but also the frequency at which they occur making the separation of the signatures change dramatically around those points.

For this type of deformation both characteristics respond similarly to the increase in capacitance with an downward shift in the difference characteristics being evident. The trans-admittance however is marginally more sensitive with changes varying between 2.9% and 11%. The characteristic impedance signatures varied between 2.4% and 8.7%

7.4 WINDING LOOSENING

Windings may become loose when they experience radial forces that stretch the clamps that hold them in place beyond their elastic limits. The result is that the winding becomes slightly unwound and the space between the turns increases. This is modeled as an decrease in the inter-turn capacitance of the winding. From the case data [15] the inter-turn separation is 3.5mm. Increases of 1mm, 2mm, 5mm and 10mm are modeled.

63

Figure 44: Actual plots for |Z$_c$| for variation in C$_{inter-turn}$

Figure 45: Percentage deviations from base plot for |Z$_c$| for variation in C$_{inter-turn}$

Winding loosening /mm	Percent change in C$_{inter-turn}$/%	Averarge measured percent change /%	Scaling factor (K)
1	21.9780	13.1926	1.6659
2	36.0360	25.0101	1.4409
5	58.4795	55.1708	1.0600
10	73.8007	95.4251	0.7734

Table 11: Actual and measured percentage changes for Z$_c$ signature for winding loosening

64

Figure 45 shows that the percentage changes are still relatively constant throughout the frequency range. However, the scaling factor between the percentage change in capacitance and the measured percentage change vary widely. This means that the percentage change that is measured is not a direct indication of how much the winding has separated as in the case for winding bulges.
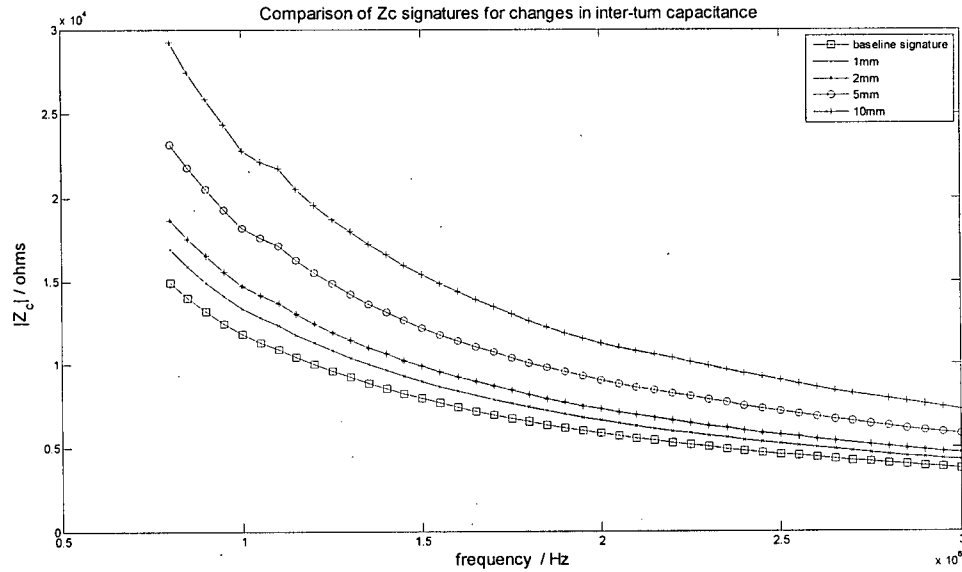

Figure 46: Actual plots for |TA| for variation in $C_{inter-turn}$

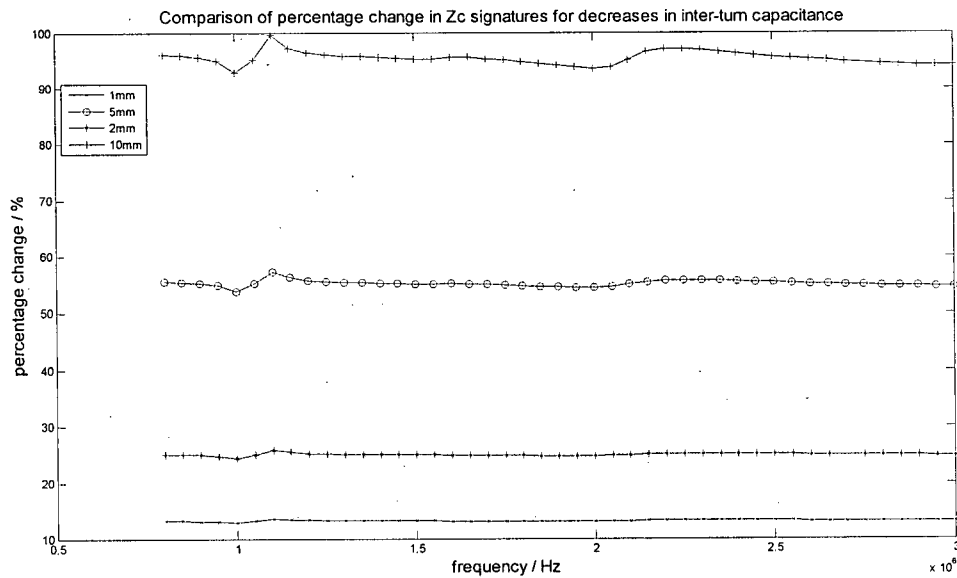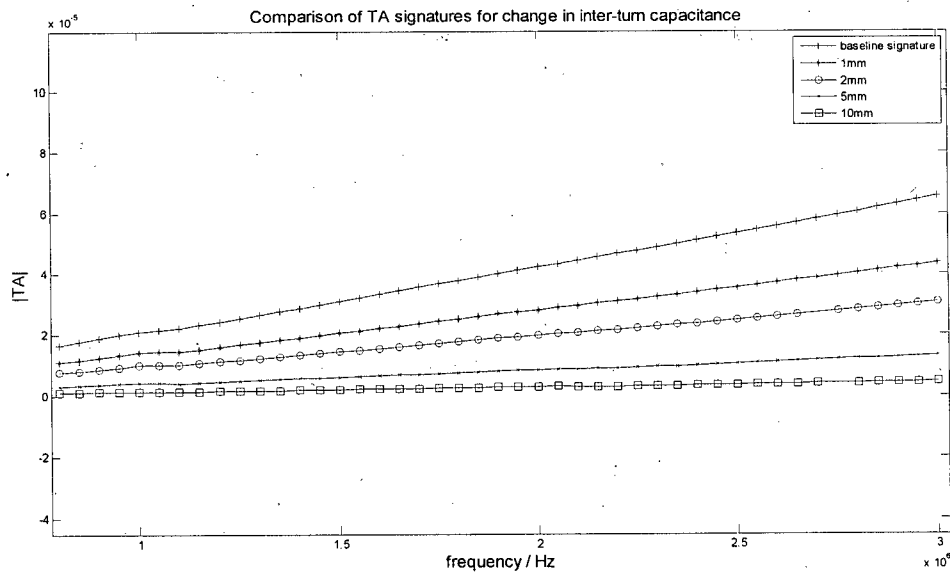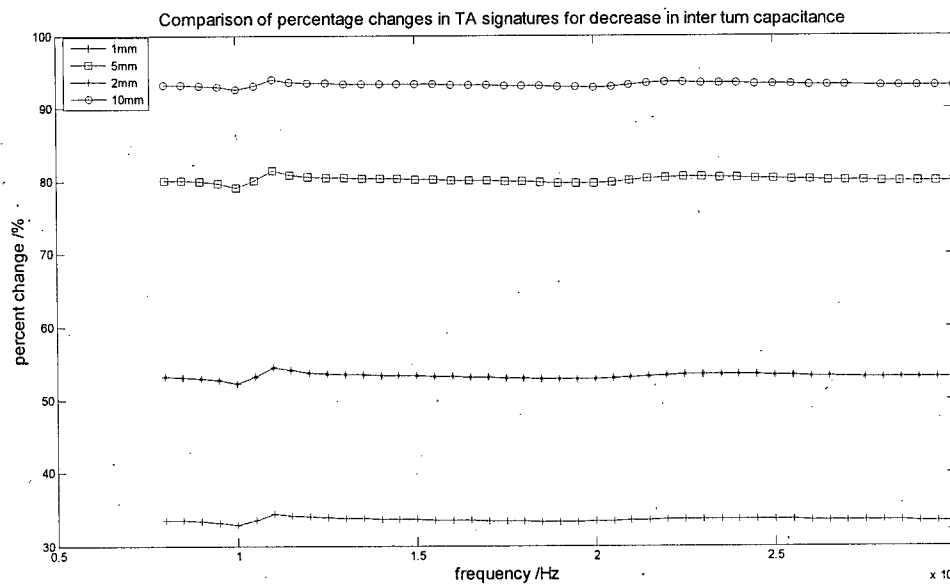**Figure 47: Percentage deviations from base plot for |TA| for variation in $C_{inter-turn}$**

Winding loosening /mm	Percent change in $C_{inter-turn}$/%	Averarge measured percent change /%	Scaling factor (K)
1	21.9780	33.5670	0.6548
2	36.0360	53.2875	0.6763
5	58.4795	80.1580	0.7296
10	73.8007	93.2565	0.7914

Table 12: Actual and measured percentage changes for TA signature for winding loosening

Here also the percentage changes remain relatively constant but the measured percentage but the scaling factors vary too much to be considered a direct indication of the winding movement.

Once again the change in capacitance has caused a corresponding unidirectional shift in both of the characteristics. This time the Zc characteristic increases since the capacitance is being decreased however the Trans-admittance characteristic decreases just as it did in the case where the capacitance to ground was being decreased. This time, the characteristic impedance signature showed a greater range in the percentage changes from approximately 13% to 95% while the transadmittance signature showed a range of 33% to 93%.

7.5 WINDING COMPRESSION

Winding compression basically creates the opposite effect to winding loosening. When a radial force is experienced, the windings are forced outward. This force is must first do the work of compressing the insulation before the force is transferred to the clamps that keep the winding in place, if the clamps are strong enough to not undergo plastic deformation then the windings may not become loose after the surge but remain in a compressed state. Since the insulation is compressed the turns are closer together and so the inter-turn capacitance increases. Simulations were performed to simulate compressions of 1mm, 2mm and 3mm with the baseline signature corresponding to a separation of 3.5mm. To simulate this, the inter-turn capacitance had to be increased proportionally.

Comparison of Zc signatures for inrease in inter turn capacitance
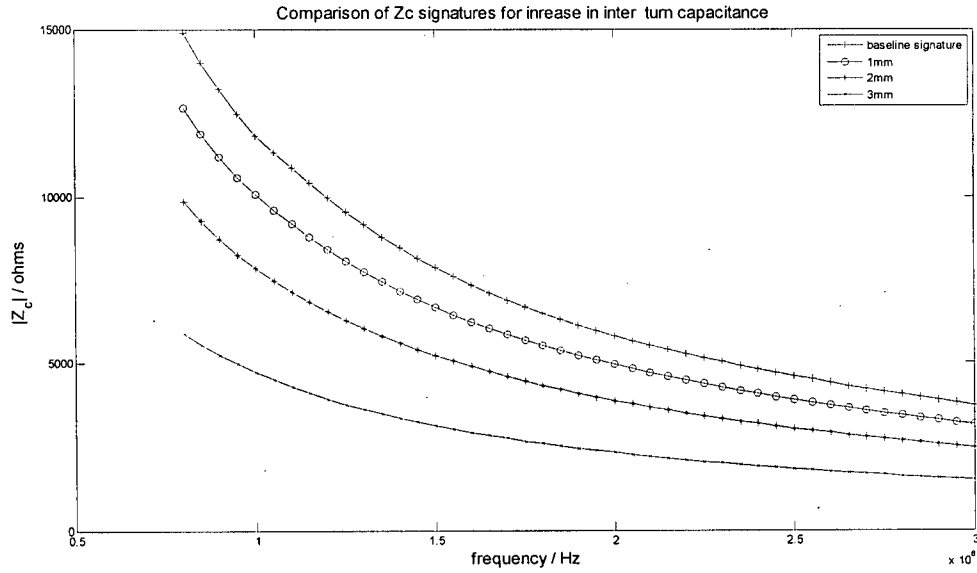
Figure 48: Actual plots for |Z$_c$| for winding compression

Comparison of percentage change of Zc signatures for increase in inter turn capacitance
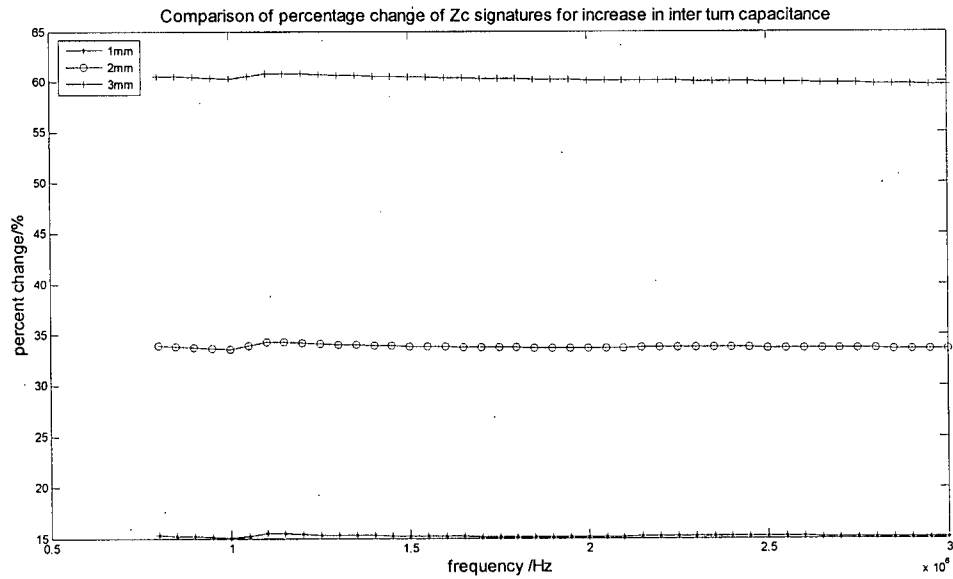
Figure 49: Percentage deviations from base plot for |Z$_c$| for winding compression

Winding compression /mm	Percent change in C$_{inter-turn}$/%	Averarge measured percent change /%	Scaling factor (K)
1	39.2157	15.2065	2.5789
2	129.0323	33.7825	3.8195
3	545.4545	60.1935	9.0617

Table 13: Actual and measured percentage changes for Z$_c$ signature for winding compression

67
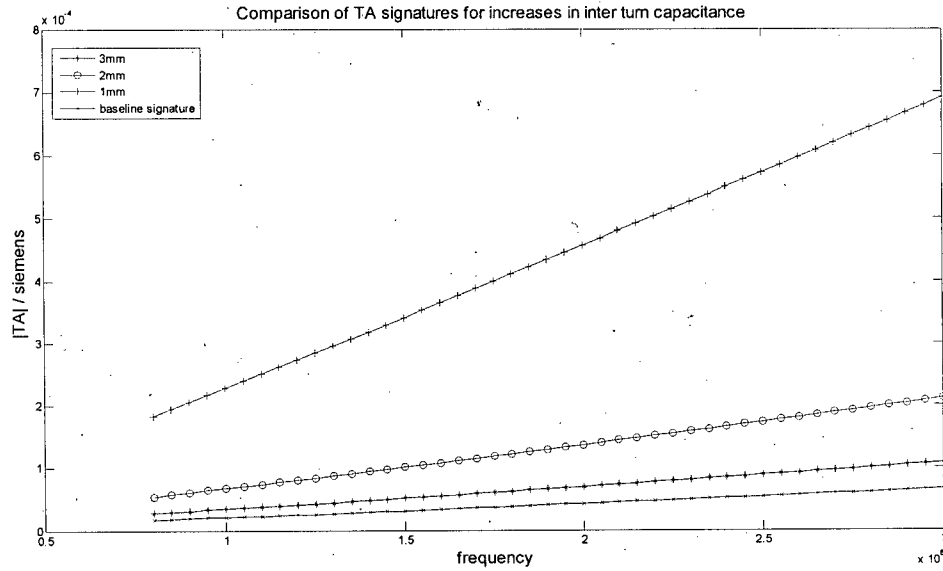
Figure 50: Actual plots for |TA| for winding compression
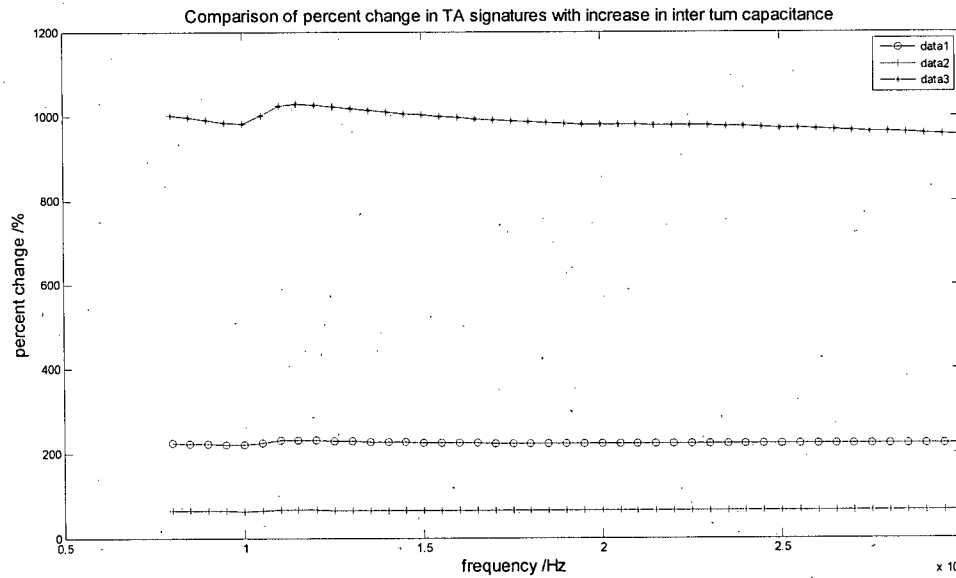
Figure 51: Percentage deviations from base plot for |TA| for winding compression

Winding compression /mm	Percent change in $C_{inter-turn}$/%	Averarge measured percent change /%	Scaling factor (K)
1	39.2157	64.8471	0.6047
2	129.0323	223.6866	0.5768
3	545.4545	986.0275	0.5532

Table 14: Actual and measured percentage changes for TA signature for winding compression

The Trans-admittance signature is extremely sensitive to this type of deformation, exhibiting between 65% and 987% deviations, while Zc exhibits a range of between 15% and 60%, which is still quite sensitive but as not sensitive as the trans-admittance.

Although this type of deformation is simply the opposite of the loosening case, the transadmittance now has a greater range than the characteristic impedance. This means that as the windings become more separated the characteristic impedance signature becomes more sensitive but if they become compressed the transadmittance will tend to become more sensitive.

CHAPTER 8: DISCUSSIONS

8.1 GENERAL

Measurements become increasingly inaccurate as multiples of the half wavelength of the signal approaches the length of the winding. At these points the input and output waves are either fully in phase or fully out of phase, causing standing waves. It has been shown that with small values of line resistance this may cause the value of Z_c to be very much larger or smaller than the expected value. Higher values of resistance seem to have a stabilizing effect on the characteristic since the energy loss caused by them reduce the similarity of the input and output waveforms. This means that at high frequencies the accuracy of the model should improve since the resistance increases proportionally with the square root of the frequency. This is why there was no evidence of discontinuities in the simulations done (the resistance becomes high in the Megahertz range).

The previous section compared the sensitivity of the characteristic impedance signature to the trans-admittance signature for different types of winding deformations. In the case of the winding bulging both showed similar levels of discrimination with the transadmittance being only marginally better. For this type of deformation, the percentage change between the baseline signature and the signature after deformation could be directly related to the actual percentage change in capacitance. This was true for both the characteristic impedance and trans-admittance signatures. However, the range of frequencies was too low to see any resonances in the transadmittance signature. Figure 52 shows a transadmittance plot up to 10MHz that illustrates the presence of resonances, while Figure 53 shows the percentage deviation over the frequency range. Figures 54 and 55 are the corresponding characteristic impedance plots.
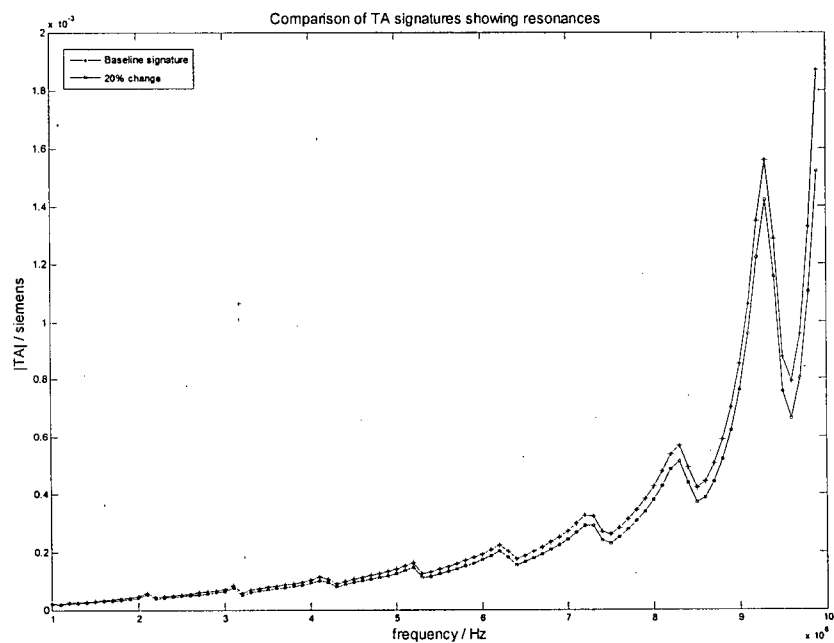
Figure 52: Transadmittance signature up to 10MHz for low line resistance
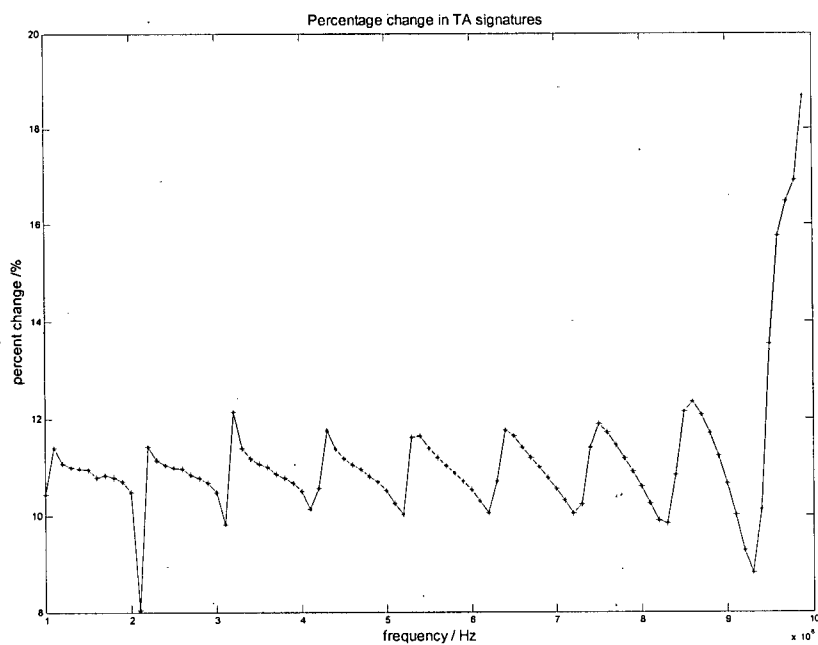
Figure 53 : Percentage change in transadmittance signatures
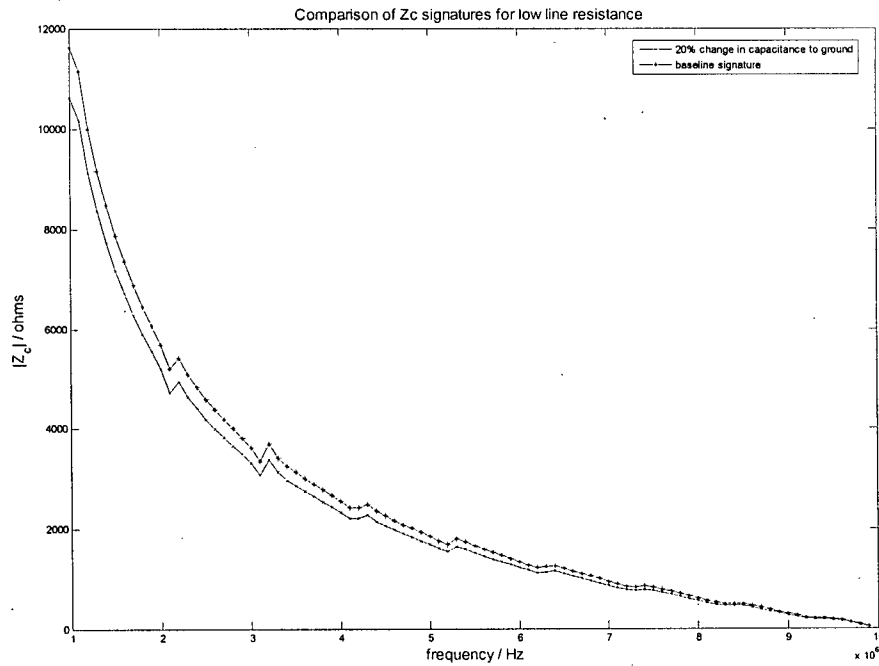
Figure 54 : Characteristic impedance signature up to 10MHz for low line resistance
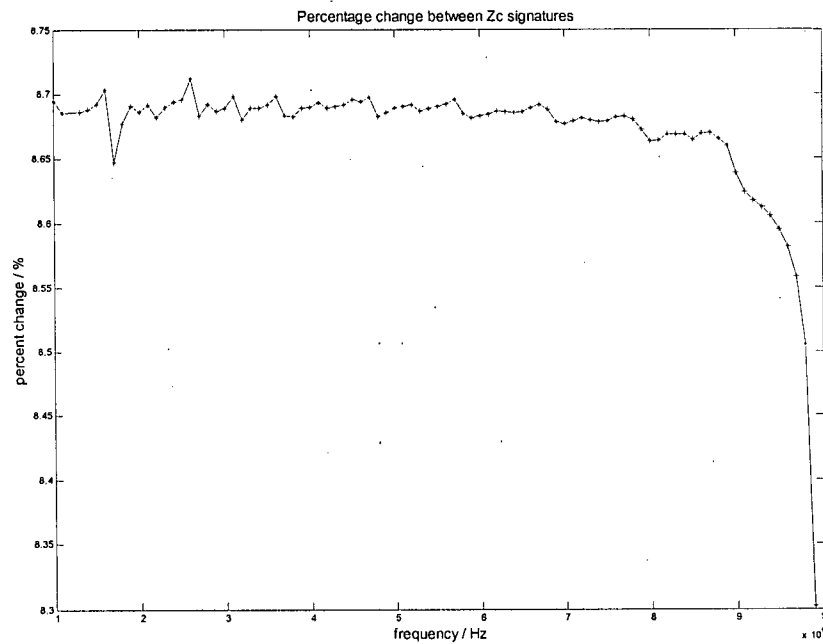
Figure 55: Percentage change in characteristic impedance signatures

Figure 53 shows a variation of about 10% with an average of approximately 11-12% deviation. This indicates that in the presence of resonances the approximately constant

72

relationship between the change in capacitance and the measured percentage difference does not exist any longer. In the case of the characteristic impedance the variation is approximately 0.5% with an average of about 8.65%. The dip toward the end is caused by standing waves produced at the characteristic frequency (10MHz) of the turns.

The data at problematic frequencies can be discarded without any loss in information for the characteristic impedance signature. This can be done first plotting all points then looking for changes in the sign of the gradient. When the gradient between two points is positive these points can be discarded. The percentage change would then exhibit even less variation indicating that the characteristic impedance can still be used.

Winding compression and loosening involved changing the same capacitance. They were simulated separately to emphasize the fact that as the windings came closer together the transadmittance signature became more sensitive and as they went further apart the characteristic impedance became more sensitive. If a record of past signatures are kept (not just one baseline signature), it may be possible to tell how the winding is moving based on how the relative magnitude of percentage deviation noticed in each signature changes.

The methods also responded differently from each other for different types of distortions. That is, a certain type of deformation may cause an increase in the trans-admittance while it causes a decrease in the characteristic impedance. Table 15 summarizes this behaviour for the three types of deformations examined.

| DISTORTION TYPE	Z_c SHIFT TYPE	TA SHIFT TYPE
BULGE	Decrease	Decrease
LOOSEN	Increase	Decrease
COMPRESS	Decrease	Increase

Table 15: type of shifts exhibited by the Z_c and TA characteristics

This combination of the characteristic impedance and trans-admittance signatures can form the beginning of a primitive winding deformation classifier. Table 15 shows that a combination of both methods allows us to uniquely classify deformation types.

Although these deformations have been dealt with separately, in practice they would occur in combination. When a radial force is experienced it is likely that the insulation would become compressed and the windings would bulge, or after the windings have expanded due to the initial force and the clamps exceeded their elastic limits the winding would become loose as well as wider.

Unsymmetrical deformations may also occur, causing some windings to bulge more than others. Deformations such as these have major implications for the capacitance matrix that is built for the model. The capacitance matrix is built based on the grid like geometry of the winding structure. If some windings expand more than others the symmetry of the grid is broken. Turns may no longer have other turns exactly above and below and on either side as shown in Figure 56 below.
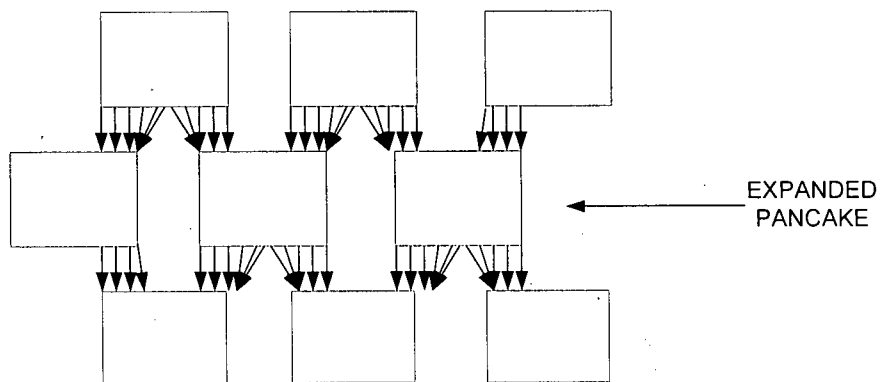
Figure 56: Unsymmetrical deformation causing turns on one pancake to link multiple turns on adjacent pancake

In situations such as these the capacitance matrix would have to be constructed to mirror this re-distribution of flux. Not only would the inter-pancake capacitances be affected but the capacitance from the winding to external structures such as the core or the tank

would no longer be equal. Windings may also become twisted such that turns no longer lie on a single plane. The model does not have the capability to deal with such complex deformations, however, the intention of condition monitoring is to pick up deformations in their early stages before such serious conditions manifest.

8.2 IMPULSE TESTS (FRA- LVI)

The original intention of the work presented was to compare the FRA-LVI method to the TLD method, however the impulse technique involves taking the Fourier transform of the input and output voltage and current waves to obtain phasor information for calculation of the trans-admittance or trans-impedance. This technique, however, is best suited for transient analyses since the Fourier transform assumes that the waveforms being analyzed are undamped whereas transients are by nature heavily damped.

Transient signal frequencies have finite energy. Since the resistance of the line increases with frequency some frequencies would be attenuated faster than others. The problem can be illustrated by taking the hypothetical situation of the finite energy of a particular frequency being dissipated after two seconds. If the sample window is large, say ten seconds, then the Fourier transform would represent this frequency by a constant amplitude signal over the entire ten seconds, even though it is only there for two seconds in actuality.

This false representation would cause an erroneous representation of the winding transadmittance. Jayalalitha [16] shows that different transfer functions are obtained for different wave shapes such as chopped waves and impulse waves. He similarly finds that the transfer functions obtained by impulse tests "ignore the finite energy deterministic nature of the input" and proceeds to use winding current as a basis for detecting partial discharge.

The signatures produced by impulse testing, however, are still valid signatures. If properly done they can be very similar to the actual transadmittance signatures gained from swept frequency methods.

75

8.3 FUTURE WORK

The model can be improved by using to a frequency dependent line model. For steady state simulations this can be done roughly on the current CP-line system by changing the velocity at every frequency step. If transient simulations are required however, then the model would have to be rebuilt using FD-line models in Microtran. The reason for this is that the line resistances are lumped at the line ends for transient simulations in the CP-line model while they remain fully distributed in the FD-Line model.

The difficulty with constructing an FD line model would be the modeling of the frequency dependent inductance. References [17] and [18] discuss the modeling of skin effect inductance by ladder networks, while [19] and [20] discuss the quantification of skin effect in a system of rectangular conductors.

The FD-line model data can also be obtained from a transformer when it is taken offline and used as a basis to construct a software representation as close as possible to the actual winding. If this, along with the modeling of deformations can be done with a sufficient level of accuracy then the model can be used to generate deformation signatures to train neural networks which can then be used to analyze the actual data from the transformer.

An additional benefit of the FD-line model is that it can be used in time domain reflectometry simulations. Time domain reflectometry can be used to pinpoint discontinuities on the winding, however because it is very sensitive to lumping and is a time domain method, the CP line can no longer be used since it lumps the line resistance for transient simulations.

Work also needs to be done in developing an intelligence based system that utilizes the data from both the characteristic impedance and transadmittance signatures to reliably diagnose the type of winding deformation.

The system accuracy was limited by the fixed column widths that Microtran used for data entry. The Microtran simulator was not designed to cater for such a complex multiphase

system which involves very small lengths of transmission lines. The model suffered limitation from both truncation errors and limited number of phases available for use in a multiphase element. These problems need to be remedied if the model is to be used in matching the measured impedances of real transformers.

CHAPTER 9: CONCLUSIONS

The model behaved as expected. Simple functions can be written to change the capacitance matrix if more complex deformation cases need to be simulated. The model can be used to find additional patterns (such as the changes in the sensitivity of the transfer functions) which can aid in the classification of deformation types.

The simulations showed that the characteristic impedance signature is comparable to the transadmittance signature in terms of ability to detect changes in winding geometry. In addition to this, in some cases it can also be used to directly quantify the winding movement.

Both methods rely on the same measured data therefore a combination of both can be used to improve the ability to distinguish between deformation types. This would be more reliable than using either signature in isolation since each signature involves a different property of the winding and so behaves differently for different types of winding displacement. In future, other signatures may easily be added to improve the analysis, provided that they do not need extra input or output data.

The model should be rebuilt using frequency dependent line elements to increase accuracy. This would also facilitate experiments using impulse methods and investigation into time domain reflectometry.

REFERENCES

[1]   Augenstein, B. Fox, W. Fischer, P. "Outsourced Monitoring and Reliability of Critical Assets", *Distributech, Serveron Corporation* p. 6. (2003).

[2]   Wang, M. Vandermaar. A.J. "Review of condition assessment of power transformers in-service", *IEEE Electrical Insulation Magazine*, Vol. 18, No. 6. pp. 12-25. (2002).

[3]   Franklin, A.C. Franklin, D.P. "The J&P Transformer Book 11th Edition: A Practical Technology of The Power Transformer", *Butterworth & Co. Ltd,* p. 629. (1983).

[4]   Jiang, Q. "Diagnostic of transformer winding movement", MaSc thesis, *University of British Columbia.*, pp. 7-8. (2004).

[5]   Tanguay, F. "Transformer Maintenance: The Cheapest Form of Insurance Part 1:The Transformer Killers", *Electricity Today* No. 1, pp. 5-9. (2002).

[6]   Sarkar, S. "The Performance Advantages of Circular Windings", *Electricity Today*, No. 5, pp. 33-35. (2001).

[7]   Christian, J. Feser, K. "Procedures for Detecting Winding Displacements in Power Transformers by the Transfer Function Method", *IEEE Transactions on Power Delivery*, Vol. 19, No. 1. pp. 214-220. (2004).

[8]   Tenbohlen, S. Ryder, S.A. "Making Frequency Response Analysis Measurements: A Comparison of the Swept Frequency and Low Voltage Impulse Methods", *13th International Symposium on High Voltage Engineering,* ISBN 90-77017-79-8, p. 4. (2003).

[9] Britton, J.A. "Transformer Maintenance and Diagnostics using Frequency Response analysis" *Electric Energy Online T&D Magazine.* http://www.electricenergyonline.com/article.asp?m=5&mag=19&article=145. (2006).

[10] Ryder, S. "Frequency response analysis for diagnostic testing of Power transformers", http://www.electricity-today.com/et/issue0601/i06_ryder.htm, *The Electricity Forum, Inc.* (2006).

[11] Marti, J.R. Srivastava K.D. Jiang, Q. "Electric winding displacement detection method and apparatus", *The University of British Columbia,* Patent pending: PAT 2796W-90. (2004).

[12] Greenwood, A. "Electrical Transients in Power Systems, Second Edition" *Wiley Interscience.* ISBN: 0-471-62058-0, p. 339. (1991).

[13] Ibid p. 333.

[14] Microtran Power System Analysis Corporation. "Reference Manual, Transients Analysis Program for Power and Power Electronic Circuits", *Microtran Power System Analysis Corporation,* p. 9. (2002).

[15] Shibuya, Y. Fujita, S. Hosokawa, N. "Analysis of very fast over-voltage in transformer windings", *IEE Proc. -Generation Transmission Distribution,* Vol. 144, No. 5, p. 5. (1997).

[16] Jayalalitha, S. "Signal Analysis techniques applied to impulse testing of transformers", PhD Thesis, *Indian Institute of Technology (Chenna),* pp.19-21. (2005).

[17]   Neikirk, D. P. Xu, G. Demkowicz, L. "Modeling and design for reduced cross talk in mixed signal analog /digital ic packages for wireless applications", *University of Texas Austin.* (1999).

[18]   Sen, B.K. "Skin Effects models for Transmission Line Structures using Generic SPICE Circuit Simulators", *IEEE Topical Meeting on Electrical Performance of Electronic Packaging*, pp. 128-131. (1998).

[19]   Weeks, W.T. Wu, L.L. McAllister, M. F. Singh, A. "Resistive and Inductive Skin Effect in Rectangular Conductors" *IBM J. Res. Develop.* Vol. 23, No. 6. pp. 652-660. (1979).

[20]   Tuncer, E. Neikirk, D.P. "Efficient Calculation of Surface Impedance for Rectangular Conductors", *Electronics Letters*, Vol. 29, pp. 2127-2128. (1993).